

DOI: 10.1093/genetics/iyaa016

Investigation

A nervous system-specific subnuclear organelle in Caenorhabditis elegans

Kenneth Pham, Neda Masoudi, Eduardo Leyva-Díaz, and Oliver Hobert*

Department of Biological Sciences, Howard Hughes Medical Institute, Columbia University, New York, NY 10027, USA

*Corresponding author: or38@columbia.edu

Abstract

We describe here phase-separated subnuclear organelles in the nematode *Caenorhabditis elegans*, which we term NUN (NUclear Nervous system-specific) bodies. Unlike other previously described subnuclear organelles, NUN bodies are highly cell type specific. In fully mature animals, 4–10 NUN bodies are observed exclusively in the nucleus of neuronal, glial and neuron-like cells, but not in other somatic cell types. Based on co-localization and genetic loss of function studies, NUN bodies are not related to other previously described subnuclear organelles, such as nucleoli, splicing speckles, paraspeckles, Polycomb bodies, promyelocytic leukemia bodies, gems, stress-induced nuclear bodies, or clastosomes. NUN bodies form immediately after cell cycle exit, before other signs of overt neuronal differentiation and are unaffected by the genetic elimination of transcription factors that control many other aspects of neuronal identity. In one unusual neuron class, the canal-associated neurons, NUN bodies remodel during larval development, and this remodeling depends on the Prd-type homeobox gene *ceh-10*. In conclusion, we have characterized here a novel subnuclear organelle whose cell type specificity poses the intriguing question of what biochemical process in the nucleus makes all nervous system-associated cells different from cells outside the nervous system.

Keywords: C.elegans; nuclear organelle; phase separation

Introduction

The interphase nucleus of a eukaryotic cell contains a large number of distinct, membraneless organelles. Best studied among these is the nucleolus, which transcribes and processes rRNAs to form ribosomes (Lamond et al. 2016). Other subnuclear membraneless organelles include splicing speckles (Galganski et al. 2017), Cajal bodies (Sawyer et al. 2016), paraspeckles (Fox et al. 2018), promyelocytic leukemia (PML) bodies (Sahin et al. 2014), histone locus bodies (Duronio and Marzluff 2017), clastosomes (Lafarga et al. 2002), and Polycomb bodies (Entrevan et al. 2016). Some subnuclear organelles only form under specific circumstances, such as nuclear stress bodies, which appear in response to heat stress (Biamonti and Vourc'h 2010). Others are developmentally regulated, such as paraspeckles which are absent during very early embryonic development (Chen and Carmichael 2009).

Most subnuclear organelles have been studied in cell lines, and few studies have systematically addressed the question of the cellular specificity of subnuclear organelles. For example, PML bodies, characterized by punctate expression of PML in the nucleus, have been assessed in an assortment of human tissues and are not found in brain and testis tissues (Gambacorta et al. 1996). Additionally, though Cajal bodies have been documented in yeast, plant, insect, amphibian, and mammalian nuclei (Gall 2000), Cajal bodies are not ubiquitously in all cell types (Ogg and

Lamond 2002; Matera 2003). Also, expression of NEAT1, a long non-coding RNA required for paraspeckle formation, is restricted only to a subpopulation of cells within a given tissue type (Nakagawa et al. 2011). However, to the best of our knowledge, no subnuclear organelle has presently been found to be restricted solely to one specific tissue type.

The limited number of diverse cell types present in Caenorhabditis elegans offers an intriguing opportunity to investigate potential tissue specificities of nuclear bodies. In his first classic C. elegans cell lineaging paper, John Sulston noted that nerve cells and their support cells are more compact than the nuclei of other somatic cells and contain a "granular nucleoplasm" (Sulston 1976). This granular nucleoplasm can readily be visualized with differential interference contrast (DIC) microscopy, also known as Nomarski microscopy. Before the advent of molecular markers, the compact, granular appearance of neuronal nuclei has served as an important indicator to assess the fate of cell lineages in specific mutant backgrounds (Chalfie et al. 1981; Ambros and Horvitz 1984). However, the cellular specificity of these granular structures has never been systematically explored and their molecular composition has remained unknown.

We became interested in analyzing these structures for two reasons. First, as stated above, the tissue specificity of any subnuclear organelles has never been systematically analyzed on a whole organism level. Second, other than the existence of long thin processes (i.e. axons and/or dendrites), there are few other morphological features that are truly panneuronal (i.e. present in all neurons), but absent in other cell types. If some subcellular organelle would indeed be tightly restricted to the nervous system, it would suggest that neurons and glia cells are unique in some aspect of nuclear biology as well. We, therefore, set out to characterize these granular structures in more detail in this study. We find that these granular structures, which we term NUN (NUclear Nervous system-specific) bodies, are phase-separated novel subnuclear organelles that are indeed entirely restricted to the nervous system and do not correspond to any previously described subnuclear organelle that we were able to examine. The function of NUN bodies—like those of many other subnuclear organelles remains unresolved, but their cellular specificity points to an aspect of nuclear function that is nervous system-specific.

Materials and methods

Caenorhabditis elegans mutant, transgenic, and genome-engineered strains

Strains were maintained by standard methods (Brenner 1974). Mutant alleles used in this study were ceh-10(ct78), ceh-10(qm127), fib-1(ok2527), hlh-3 (tm1688), hpl-1(n4317), hpl-2(tm1489), lin-4(e912), mes-2(bn11), met-2(n4256), ncl-1(e1865), nono-1(gk1206), set-11(ok1691), set-25(n5021), smn-1(ok355), smo-1(ok359), ubc-18(tm5426), unc-3(e151), and unc-86(m846), which we all acquired from the CGC strain repository. The rsp-4(tm837) allele was acquired from the National Bioresource Project for the Nematode. In addition, SunyBiotech generated a deletion allele, wac-1.1, wac-1.2(syb2587), that eliminates the wac-1.1 and wac-1.2 loci.

Previously described transgenes used in this study are:

```
ccIs4251 [(pSAK2) myo-3p::GFP::LacZ::NLS + (pSAK4) myo-
3p::mitochondrial GFP + dpy-20(+)] I (Fire et al. 1998)
drSi13 [hsf-1p::hsf-1::GFP::unc-54 3'UTR + Cbr-unc-119(+)] II
(Morton and Lamitina 2013)
lqIs4 [ceh-10p::GFP + lin-15(n765)] X (Lundquist et al. 2001)
mcIs17 [lin-26p::GFP + rol-6(su1006)] (Bosher et al. 1999)
nsIs213 [egl-6::gfp] X, kindly provided by Shai Shaham
nsIs698 [mir-228p::NLS::RFP] (Katz et al. 2019)
osEx240 [bet-1p::bet-1::GFP + unc-76(+)] (Shibata et al. 2010)
otEx1028 [lin-49::gfp + rol-6(su1006)] (Chang et al. 2003)
otEx1325 [lsy-2::gfp + rol-6(su1006)] (Johnston and Hobert 2005)
otIs33 [kal-1::gfp; pBX] IV (Bülow et al. 2002)
otIs107 [ser-2p::GFP + lin-15(+)] (Tsalik et al. 2003)
otIs355 [rab-3p::NLS::RFP] IV (Stefanakis et al. 2015)
otIs396 [ace-1prom2::NLS::tagRFP] (Serrano-Saiz et al. 2013)
vrEx6 [nst-1p::nst-1::GFP::nst-1 3' UTR + unc-119(+)] (Kudron and
```

Previously described CRISPR engineered endogenously tagged protein alleles used in this study are:

```
smn-1(rt280[smn-1::gfp]) I (O'Hern et al. 2017)
exc-7(ot970[exc-7::qfp::3xflaq]) II (Pham and Hobert 2019)
mes-2(ax2059[mes-2::gfp]) II (Paix et al. 2014)
hpl-2(ot860[hpl-2::mKate2]) III (Patel and Hobert 2017)
met-2(qw1419[met-2::FLAG::TEV::mCherry]) III (Delaney et al.
unc-86(ot893 [unc-86::mNeonGreen::AID]) III (Serrano-Saiz et al.
pgl-1(gg547[pgl-1::3xflag::tagRFP]) IV (Wan et al. 2018)
dmd-4(ot934 [dmd-4::gfp]) X (Bayer et al. 2020)
```

```
hpl-1(ot841[hpl-1::mKate2]) X (Patel and Hobert 2017)
```

Additionally, CRISPR/Cas9-mediated modification of the genome was used to generate endogenously tagged protein strains using hybrid PCR-based donors (Dokshin et al. 2018). Briefly, L4 hermaphrodites were used for gonad injection of a mix containing: Streptococcus pyogenes Cas9 protein (250 ng/µl, IDT, Coralville, IA, USA), tracrRNA (100 ng/µl, IDT), locus-specific crRNA (56 ng/ μl, IDT), dsDNA donor cocktail (300 ng/μl), and PRF4::rol-6(su1006) plasmid (40 ng/µl). The following alleles were generated for this

```
rpt-3(ot1017[rpt-3::qfp::3xflaq]) III
nono-1(ot1018[nono-1::qfp::3xflaq]) III
fib-1(ot1036[fib-1::qfp::3xflaq]) V
ama-1(ot1037[gfp::3xflag::ama-1]) IV
smo-1(ot1038[smo-1::qfp::3xflaq]) I
fust-1(ot1039[fust-1::qfp::3xflaq]) II
rpc-1(ot1041[rpc-1::gfp::3xflag]) IV
fox-1(ot1081[fox-1::qfp::3xflaq]) X
rsp-4(syb2575[rsp-4::qfp]) II. This strain was generated by
Sunvbiotech.
set-11(syb3003[set-11::gfp]) II. This strain was generated by
Sunybiotech.
```

Additionally, for a canal-associated neuron (CAN)-specific reporter strain, pKP1 was made by subcloning 541-bp pks-1 promoter fragment (-541 to -1 from ATG) (Shou et al. 2016; Lorenzo et al. 2020), into pNS2, a TagRFP containing plasmid. The construct (200 ng/µl) was injected into OH16460 (fib-1(ot1036[fib-1::gfp])/+ V) hermaphrodites along with and PRF4::rol-6(su1006) plasmid (70 ng/µl) as injection marker. From this, three lines were generated. Images presented in this study were from otEx7584.

Microscopy and imaging

Worms were anesthetized using 50 mM of sodium azide (NaN₃) in M9 and mounted on 5% agarose on glass slides. Images were acquired using an Axio Imager.Z1 microscope and a LSM880 confocal microscope (Zeiss, Thornwood, NY, USA).

Micrographs of single nuclei were enlarged using the Scale function with bicubic interpolation in Fiji/Image J.

For long-term imaging of neuronal nuclei, worms were mounted on 5% agarose on glass slides and anesthetized with 0.01% levamisole (Sigma-Aldrich, St. Louis, MO, USA) as previously described (Wong et al. 2011).

NONO-1::GFP intensity was measured using Zen 3.1 Blue software (Zeiss). The acquisition parameters were maintained constant among all samples (same pixel size and laser intensity). For this experiment, head hypodermal nuclei were measured. Fluorescence intensity was measured in the focal plane of the hypodermal nuclei with the strongest NONO-1::GFP expression within the z-stack. Four circular regions of interest per nucleus were used to sample intensity of NONO-1::GFP in the nucleoplasm where puncta were absent. For each worm, a single, circular region of interest was also used to measure the background intensity of the worm's autofluorescence in an adjacent area where there were no nuclei.

Surface plot generation

Surface plots of the interiors of the neuronal and hypodermal nuclei were generated drawing a square within the nucleus and plotting the gray levels from the DIC channel using the built-in function in Fiji/Image J.

Hypertonic exposure

rol-6(su1006) worms were placed in a 225 mM solution of NaCl and 25 mM of sodium azide (NaN₃) in M9, mounted on 5% agarose on glass slides and imaged as described in Microscopy and imaging.

Temperature sensitivity test

Synchronized L4 worms were grown at 20°C. Plates were moved to a 35°C incubator for an hour and then subsequently imaged as described in Microscopy and imaging.

α-Amanitin treatment

α-amanitin treatment protocol was adapted from a previously published protocol (Lee et al. 2016). Briefly, synchronized L4 worms were incubated in $100\,\mu\text{g/ml}$ α -amanitin (Cayman Chemical Company, Ann Arbor, MI, USA) in M9 for 4h on a rotator. Then, worms were imaged as described in Microscopy and imaging.

Live DNA and RNA staining

Worms were incubated at 20°C in 100 µg/ml Hoechst 33342 (Thermo Fisher Scientific, Waltham, MA, USA) in M9 or $10\,\mu M$ SYTO RNASelect Green Fluorescent Cell Stain (Thermo Fisher Scientific) in M9 for 3h for DNA and RNA staining, respectively. Then, worms were imaged as described in Microscopy and imaging.

Data analysis and availability

Strains are available at the Caenorhabditis Genetics Center or upon request. The authors state that all data necessary for confirming the conclusions presented in the article are represented fully within the article. Data were analyzed and presented with the R programming environment. Two-sample Student's t-tests were used along with post hoc Bonferroni corrections when more than two pairwise statistical tests were performed, except in Figure 5C comparing the count of NONO-1::GFP(+) foci. There, Wilcoxon signed-rank test was used.

Supplementary material is available at figshare DOI: https:// doi.org/10.25386/genetics.13235102.

Results

Cellular specificity of a granular nucleoplasm

We first set out to comprehensively examine and document the cell type specificity of granular nucleoplasm in adult animals. In accordance with Sulston's (1976) original observation that neuronal and glial nuclei have a granular nucleoplasm, we find that all examined neuronal and glial nuclei (with the exception of the amphid sheath glia, an unusual glial cell type with a very large nucleus) have a granular nucleoplasm in the adult animal but other cell types, such as muscles, intestine, or epidermal cells, do not (Figure 1A and B).

Outside of the nervous system, Sulston (1976) also noted that muscle nuclei have a granular nucleoplasm only during the L1 stage. Prompted by that observation, we examined nuclei of various cell types at the L1 stage. Other than for intestinal nuclei, we broadly observed a granular nucleoplasm in nuclei of many cell types (Figure 1C). However, at the L1 stage, the occurrence of a granular nucleoplasm is variable and inconsistent in most cell types, but there is always a granular nucleoplasm in neuronal and glial nuclei (Figure 1D). By the second larval stage, nuclear granules have completely disappeared from all non-neuronal and non-glial cells. In addition to neurons and glia, nuclear granules are also consistently observed in the head mesodormal cell (hmc), which is a neuron-like cell in the head of the worm with many small projections and is positive for the neurotransmitter GABA (Gendrel et al. 2016). However, hmc contains fewer granules than other neuronal or glial cells

We examined different cell types within the nervous system, covering distinct neuron and glia types, marked with afp or rfp, throughout the entire nervous system (Figure 2A). We find that there is no more variability in the number of nuclear granules between different cell types in the nervous system than there is variability between animals (Figure 2B). Moreover, the granule counts do not obviously correlate with the lineage, neurotransmitter type, or functional type of the neurons (Figure 2, A and B). Furthermore, the nervous system specificity of these nuclear granules is not simply a relation to the relatively small size of neurons. While soma size of neurons is indeed much smaller than that of other somatic cell types, nuclei size is remarkably similar across somatic cell and tissue types, averaging about 2.5 µm in diameter (the only exception is intestinal nuclei which are 50% larger) (Long et al. 2009). The notably smaller number of nuclear granules in the pharyngeal M4 neurons compared to non-pharyngeal neurons does not positively correlate with nuclear size. For example, hermaphrodite-specific neuron (HSN) contains about twice as many nuclear granules as M4 (Figure 2), but the HSN nucleus is not larger than the M4 nucleus (as assessed by measuring nuclear size with the NeuroPAL landmark strain; Yemini et al. 2021).

Time lapse imaging reveals that the number of nuclear granules in neuronal nuclei varies over time (Figure 3A). We have not been able to observe fusion nor fission events and therefore believe that these granules can dynamically assemble and disassemble. To study the nuclear granules' genesis, we live imaged developing embryos. We first observed nuclear granules minutes after the terminal division of cells of whatever lineaging history in the embryo (Figure 3B and C). We conclude that nuclear granules rapidly assemble after the cells exit the cell cycle, but, as stated above, are maintained exclusively in neurons and glia cells past the L2 stage.

Neurons that arise by transdifferentiation from other cell types also contain nuclear granules. During development, the epithelial cell, Y, becomes to a motor neuron, PDA, and upon transdifferentiation to PDA, nuclear granules emerge (Jarriault et al. 2008). Ectopic transdifferentiation of germs cells to neurons is also accompanied by the appearance of characteristic granular nucleoplasm (Ciosk et al. 2006; Tursun et al. 2011). Furthermore, in mutants where a neuron, I4, adopts a muscle fate, the nuclear granules are no longer present (Luo and Horvitz 2017). Thus, the granular nucleoplasm is a distinguishing characteristic of neu-

Nervous system-specific nuclear granules behave like membraneless organelles

We sought to biophysically assay the integrity of these nervous system-specific nuclear granules. We find that the nuclear granules of L4 animals are liable to dissolution minutes upon exposing animals to a hypertonic salt solution (Figure 4A), a common feature of phase-separated membraneless organelles (Berry et al. 2015; Gibson et al. 2019; King and Petry 2020). Furthermore, heating the animals by incubation at 35°C for an hour, resulted in a decrease in nuclear granules number as well as an increase in

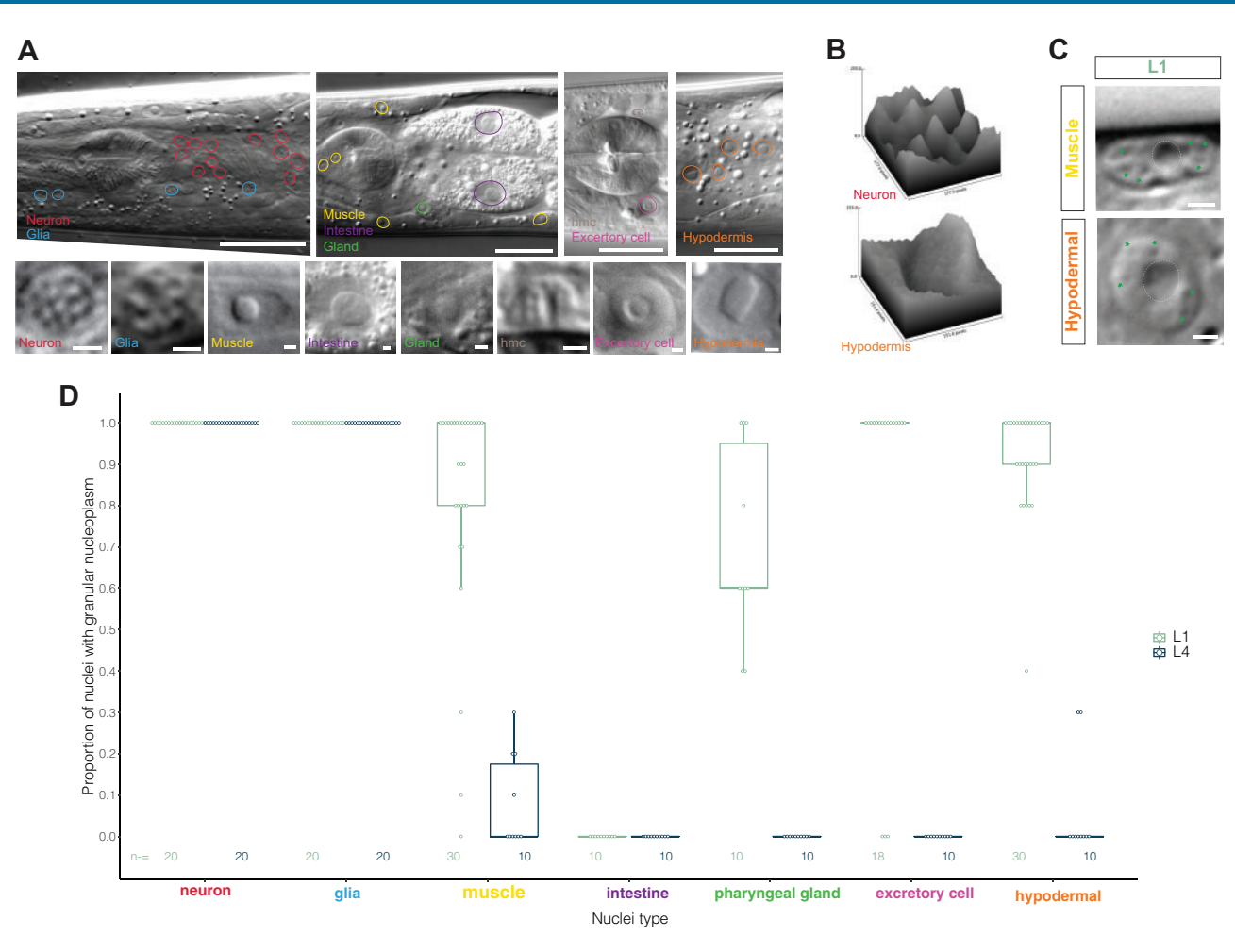


Figure 1. A persistent, granular nucleoplasm is a nervous system-specific feature. (A) Nomarski micrographs of an adult animal and its nuclei. Glia were identified with the fluorescent transgene nsls698 [mir-228p::NLS::RFP], muscle with ccls4251 [myo-3p::GFP; dpy-20(+)], hypodermal marker mcls17 [lin-26p::GFP + rol-6(su1006)] and other cells were identified by their characteristic locations. Note that all mir-228p::NLS::RFP(+) glia show a granular nucleoplasm, with the sole exception of the amphid sheath cells, an unusual glial cell with a very large soma. Bar indicates 20 μm in top row and 1 μm in single-nuclei micrographs. (B) Surface plots of the gray levels from the DIC channel of the interiors of the neuronal and hypodermal nuclei in panel A generated using Image J. (C) Nomarski micrographs of nuclei outside the nervous system that sometimes have a granular nucleoplasm at an earlier larval stage. Nucleolus outlined and green arrows point to the granules. Bar indicates 1 μm. (D) The granular nucleoplasm is only robustly observed in neurons and glia and it persists exclusively in neurons; proportion of nuclei with a granular nucleoplasm of each cell type in L1 and L4 animals. 1 = 100% of examined cells display granular nucleoplasm. Each dot represents one animal examined. For neuron, glia, muscle, intestine, and hypodermis, 10 nuclei were examined from each animal. For the pharyngeal gland, five nuclei were examined per animal. For the excretory cell, the sole excretory cell nucleus of that animal was scored. The glia nuclei scored are around the anterior bulb of the pharynx. Thick bars show median, boxes represent quartiles, and vertical lines show range. Number of animals observed included.

average nuclear granule size, reminiscent of Ostwald ripening or growth by coalescence as a result of increased Brownian motion (Berry et al. 2015) (Figure 4, A and B, C). These sensitivities to perturbations in salt concentration and temperature taken with the visibility of these granules with DIC microscopy are consistent with the nuclear granules existing as coacervate droplets within a dilute nucleoplasm phase.

To further analyze the phase-separated nature of these granules, whole animals were immersed in 1,6-hexanediol solution, a treatment known to disrupt phase-separated membraneless organelles, including nucleoli (Kroschwald et al. 2017; Abraham et al. 2020). Treatment with hexanediol indeed resulted in the dissolution of the nucleoli in intestine and germ cell nuclei, but only in a rare proportion of animals. However, the nucleoli of hypodermal and muscle remained unaffected, and therefore the lack of an effect that we see on neuronal nuclear bodies is not interpretable. Presumably, different tissue types differ in their ability to absorb 1,6-hexanediol.

NUN bodies are not nucleoli

Nucleoli are phase-separated membraneless organelles that are easily visualized by Nomarski microscopy in non-neuronal cell types, such as hypodermal cell nuclei, where nucleoli form a single large subnuclear structure (Figures 1A and 5A). We considered the possibility that nervous system-specific nuclear granules may be fragmented nucleoli and that such fragmentation may be a nervous system-specific process. We tested this possibility in two different ways. First, we examined two distinct nucleolar markers, a CRISPR/Cas9-genome engineered fib-1::gfp allele that we generated and an nst-1::gfp transgene (Kudron and Reinke 2008). We find that in each nucleus of L4 stage animals, there is one GFP(+) nucleolus. In neurons, only one of the nuclear granules co-localizes with GFP signal from the nucleolar markers (Figure 5A). Second, we used ncl-1(e1865) mutants, in which nucleoli become significantly enlarged (Hedgecock and Herman 1995). We found that each neuronal nucleus had one enlarged nucleolus, but other nuclear granules remained (Figure 5, A and

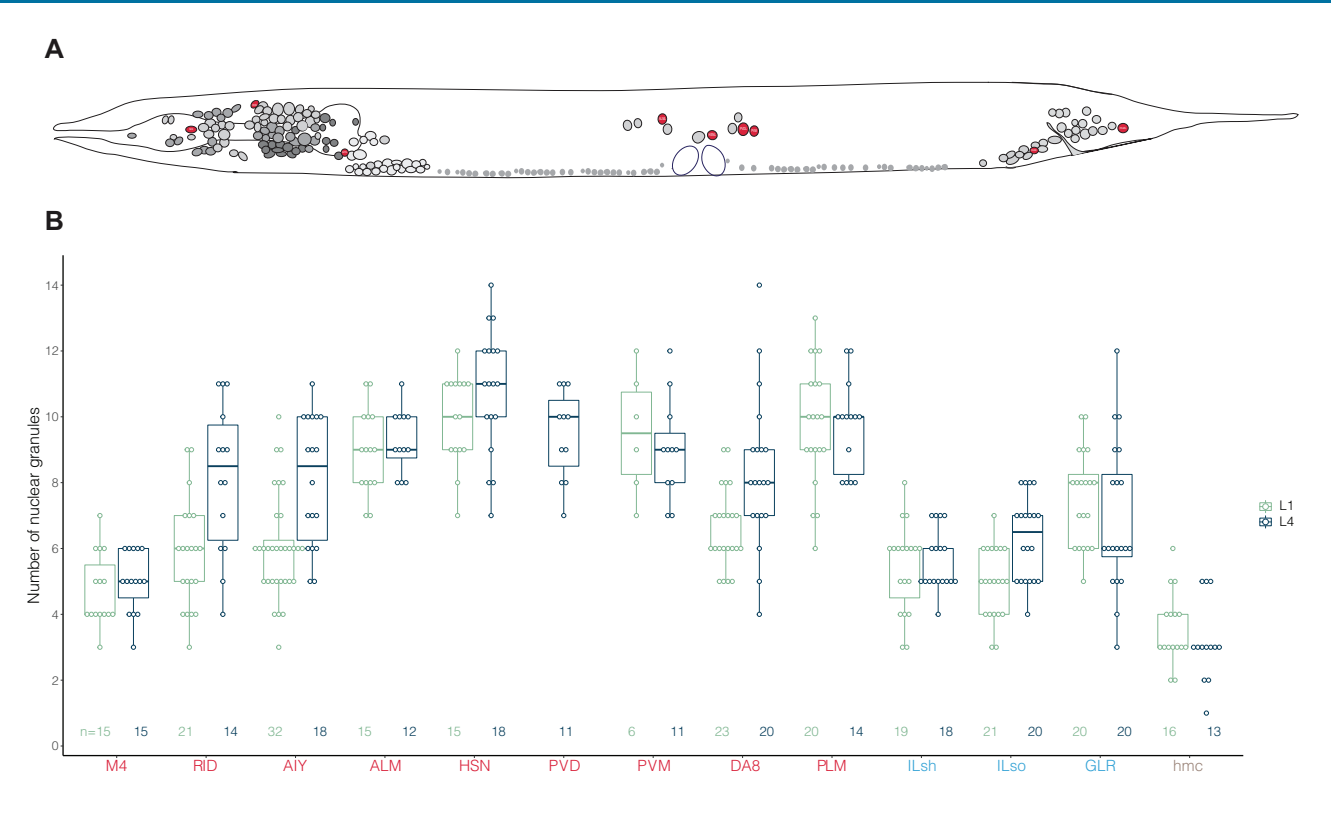


Figure 2. Number of granules in the nuclei of the nervous system . (A) Schematic localization of neurons in which we quantified the occurrence of nuclear granules. (B) The number of nuclear granules does not show any specific correlations across neuronal cell types or glia observed at the L1 and L4 larval stages. Each dot represents one nucleus examined. Neurons and glia were identified with the following gfp markers in the background:

RID and AIY neurons—lqIs4 [ceh-10p::GFP + lin-15(n765)] X

ALM, HSN, PVD, and PML neurons-unc-86(ot893 [unc-86::mNeonGreen::AID]) III

DA8 neuron—otIs107 [ser-2p::GFP + lin-15(+)]

ILsh and Ilso gia-nsIs698 [mir-228p::NLS::RFP]

GLR glia—nsIs213 [egl-6::gfp] X, kindly provided by Shai Shaham

hmc—dmd-4(ot934 [dmd-4::gfp]) X

Thick bars show median, boxes represent quartiles, and vertical lines show range.

B). We compared the count of the nuclear granules in two neuron classes in wild-type and ncl-1 mutant animals. For the wild-type count, we subtracted one from the number of nuclear granules to account for the nucleolus. The number of nuclear granules was not statistically significant different in the AIY or RID neurons of wild-type and ncl-1 mutant animals (Figure 5B). We conclude that one nuclear granule is the nucleolus. As other nuclei outside of the nervous system only have one nuclear granule, the one nucleolus, in their nuclei, we call the remaining nervous systemspecific nuclear granules NUN (NUclear Nervous system-specific) bodies.

Analysis of the existence of other well-characterized subnuclear organelles in C. elegans and their relationship to NUN bodies

Moving beyond nucleoli, we considered other wellcharacterized subnuclear organelles. We assembled a list of well-characterized subnuclear organelles and asked whether (1) the C. elegans genome encodes homologous constituents of such subnuclear organelles and (2) if so, whether they colocalize with NUN bodies (Supplementary Table S1). Reciprocal BLAST searches reveal that C. elegans does not encode the core constituents to a number of distinct subnuclear organelles (Supplementary Table S1). For example, there is neither easily recognizable sequence homolog of coilin, the core constituent of Cajal bodies, nor a PML protein homolog, the core constituent of PML bodies. There are also no C. elegans homologs of the three core components of histone locus bodies (FLASH, U7 snRNP, and NPAT). However, as summarized Supplementary Table S1, there are C. elegans orthologs of the nuclear gem constituent SMN1 (encoded by C. elegans smn-1), of the core constituents of splicing speckles (e.g. SC35/SRSF2, encoded by rsp-4, or SRF1, encoded by rsp-3) and of paraspeckle proteins (NONO/PSPC1/SFPQ, and RBM14, encoded by nono-1 and mp-1, respectively). We examined the subnuclear localization of these orthologs and further examined the subnuclear localization of a number of additional candidate proteins, as listed in Supplementary Table S1. To this end, we used available reporter lines or generated our own CRISPR/ Cas9-genome engineered reporter alleles. We found essentially three categories of expression and localization: we observed no nuclear expression of the C. elegans protein, diffuse nuclear localization, or localization to subnuclear foci. However, whenever we found such focal localization, it did not overlap with NUN bodies. The detailed results are described in the next few sections.

Caenorhabditis elegans have NONO-1(+) paraspeckles, but they are not NUN bodies

The clearest example of a subnuclear localization pattern, but lack of overlap with NUN bodies was observed with NONO-1, the

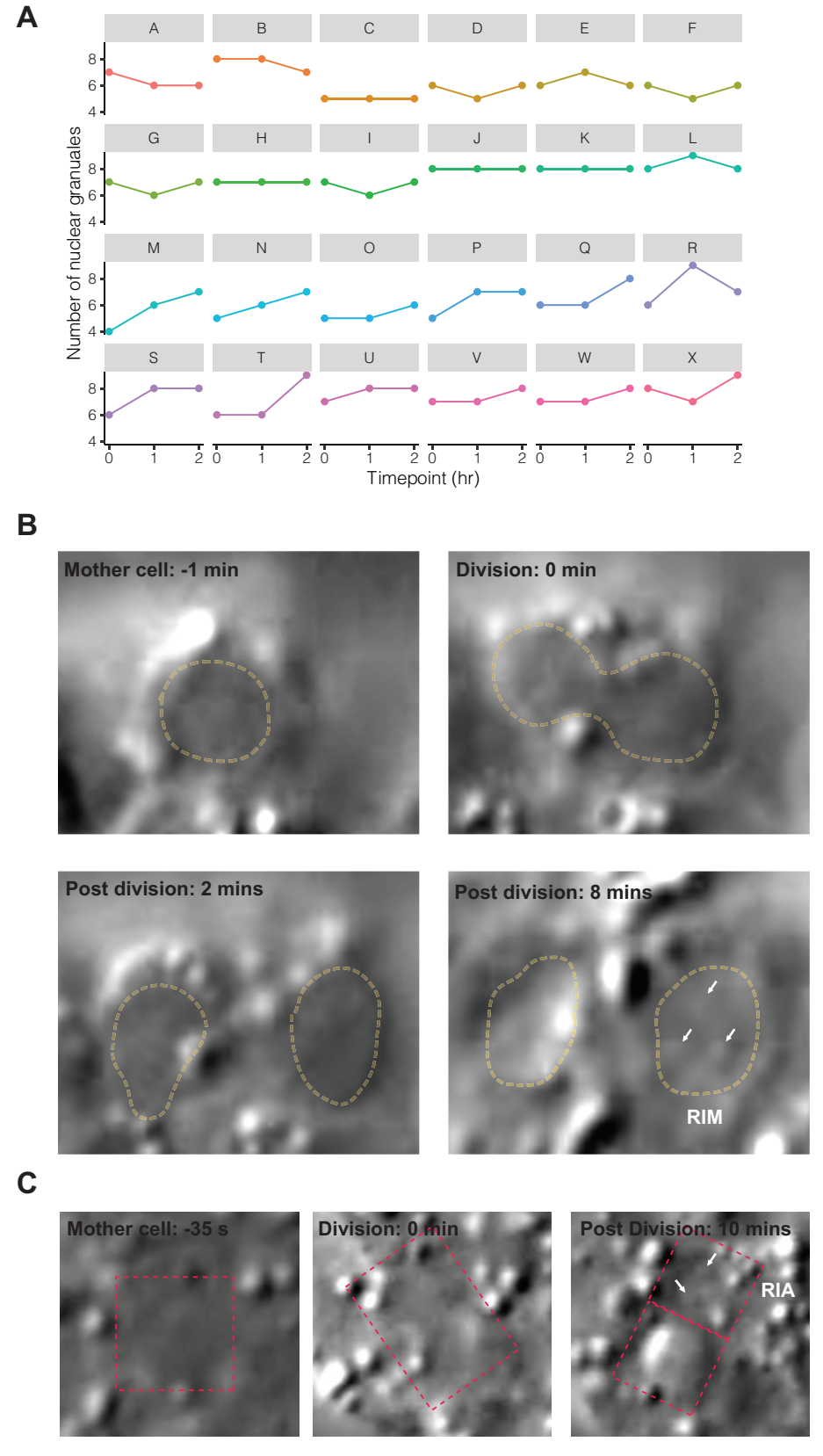


Figure 3. Dynamic nature of nuclear granules. (A) Count of nuclear granules in 24 tail neurons at three time points, over 2 h. (B) Stills from a recording of RIM terminal division. White arrows point to nuclear granules. Nuclei outlined with dashed lines. (C) Stills from a recording of RIA terminal division. White arrows point to nuclear granules. Dashed squares indicate nuclei.

C. elegans ortholog of the key constituent of paraspeckles (Knott et al. 2015; Fox et al. 2018). Through endogenous GFP tagging of NONO-1 through CRISPR/Cas9 genome engineering, we found

that NONO-1::GFP localizes to discrete nuclear foci in nuclei, but the NONO-1::GFP puncta do not overlap with NUN bodies (Figure 6A). Nuclear NONO-1::GFP foci are also not restricted to

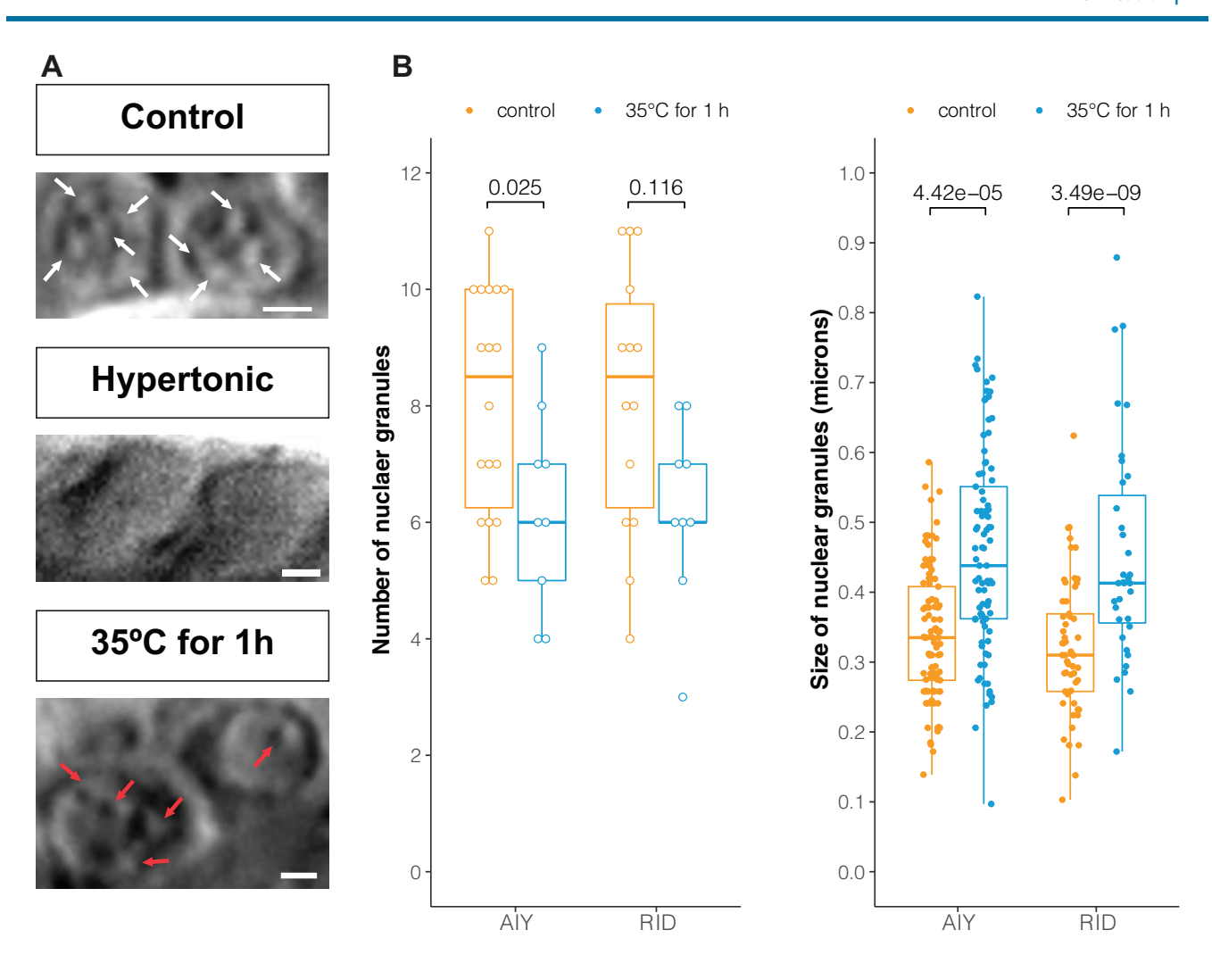


Figure 4. Nuclear granules behave as phase-separated subcompartments of the nucleus. (A) Nomarski micrographs of the granular nucleoplasm of neurons disrupted upon changes to the ionic strength and temperature. Bar indicates 1 µm. White and red arrows point to nuclear granules. (B) Number of nuclear granules in AIY and RID neurons in animals exposed to 35° for 1 h. Thick bars show median, boxes represent quartiles, and vertical lines show range. Two-sample Student's t-tests were used along with post hoc Bonferroni correction. (C) Size of nuclear granules in AIY and RID neurons in animals exposed to 35°C for 1 h. Thick bars show median, boxes represent quartiles, and vertical lines show range. Two-sample Student's t-tests were used along with post hoc Bonferroni correction.

neuronal nuclei, but are observed in many nuclei of other cell types, including gland, muscle, intestine, hypodermis, and germ cells (Figure 6, B, D, and E). We find that these foci are present neither in one-cell and two-cell embryos in utero (data not shown) nor in early embryos of 26-44 cells (Figure 6C, top panel). Foci form in prebean embryos during gastrulation (Figure 6C, bottom panel); and by the twofold stage, foci are broadly observed in the nuclei of many cell types (data not shown).

We find these NONO-1(+) speckles to be dependent on RNA polymerase II transcription as treatment with α -amanitin disperses the majority of NONO-1::GFP puncta (while leaving NUN bodies unaffected), leading to an increased diffuse NONO-1::GFP signal in the nucleoplasm (Figure 5, D-F). In line with other studies of mammalian paraspeckles (Sasaki et al. 2009; Sunwoo et al. 2008), this result is consistent with the integrity of the NONO-1::GFP foci being dependent on transcription of a non-coding RNA. We conclude that contrary to previous assertions about the restriction of paraspeckles to mammals (Nakagawa et al. 2011), C. elegans contains paraspeckles.

PML bodies, clastosomes, nuclear gems, Polycomb bodies, and splicing speckles are not **NUN** bodies

Even though there is no PML protein ortholog encoded in the C. elegans genome, we nevertheless analyzed the localization pattern of C. elegans SMO-1, which codes for the SUMO protein which in vertebrates localizes to PML bodies (Shen et al. 2006). We GFP-tagged SMO-1 through CRISPR/Cas9 genome engineering. We did not detect any expression in neuronal nuclei, but detected very dim SMO-1::GFP expression in head and bright expression in the gonad of adult animals (Figure 7A and Supplementary Figure S1A).

Clastosomes are a subnuclear organelle identified through staining against a component of the 26S proteasome, RPT3/PSMC4 (Lafarga et al. 2002). We tagged the C. elegans ortholog RPT-3 using CRISPR/Cas9 genome engineering and detected no RPT-3::GFP expression in neuronal nuclei (Figure 7A). Instead, RPT-3::GFP shows cytoplasmic expression in neurons and cytoplasmic and nucleoplasmic expression in other cell types in the adult animal (Supplementary Figure S1B).

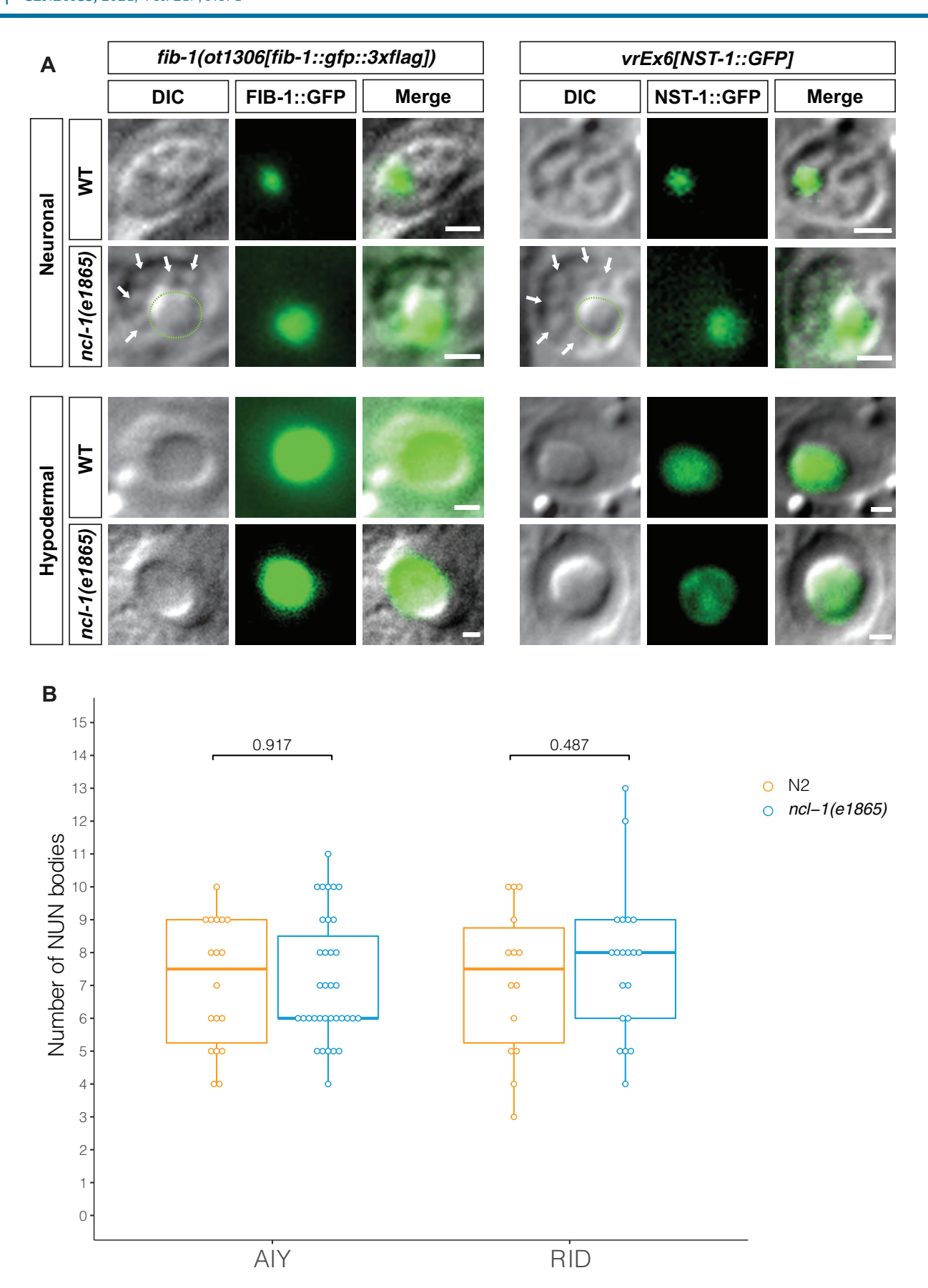


Figure 5. NUN bodies are not nucleoli. (A) Nomarski micrographs of neuronal and hypodermal nuclei with FIB-1::GFP (fib-1(ot1036[fib-1::gfp::3xflag]) and NST-1::GFP (vrEx6) in wild-type and ncl-1(e1865) animals. Nucleolus outlined in green and remaining granules pointed to with white arrows. Bar indicates 1 µm. (B) Number of NUN bodies in AIY and RID neurons of wild-type and ncl-1(e1865) animals. Thick bars show median, boxes represent quartiles, and vertical lines show range. Two-sample Student's t-tests were used along with post hoc Bonferroni correction.

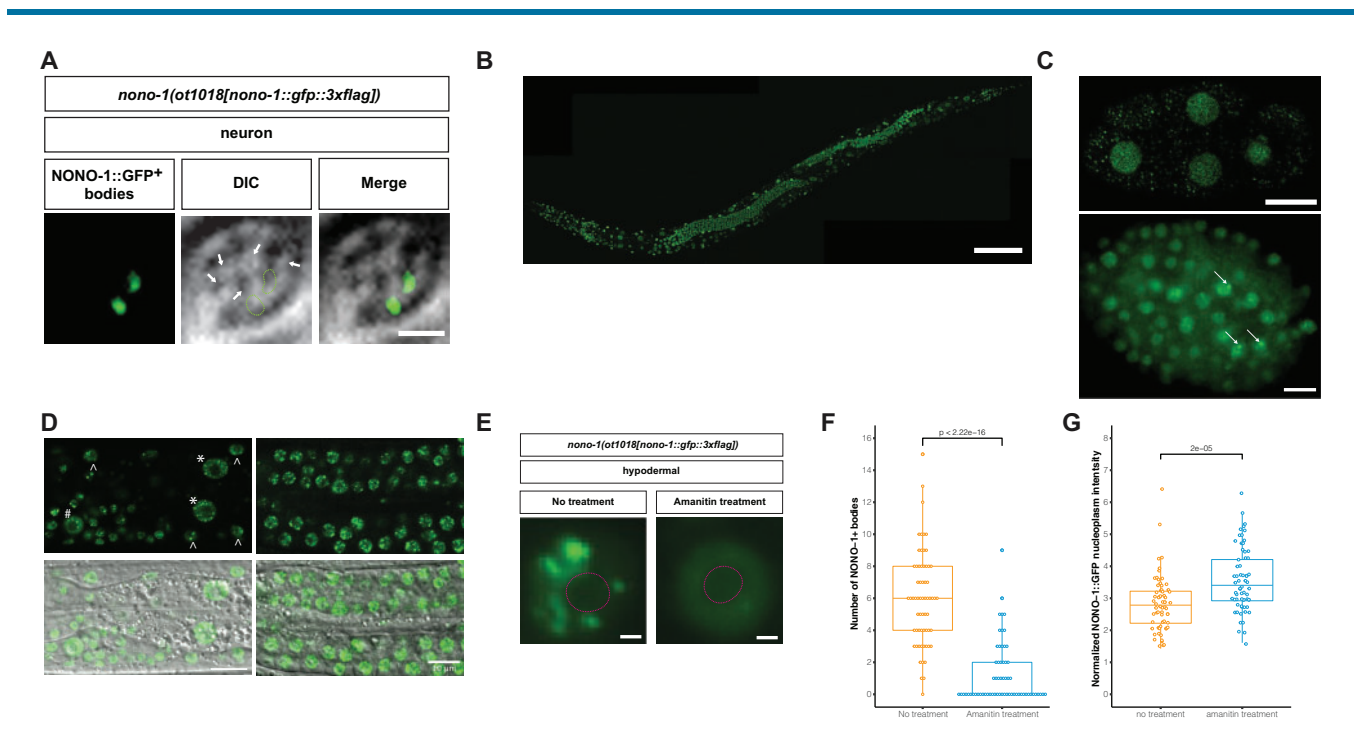


Figure 6. Caenorhabditis elegans has paraspeckles, but NUN bodies are not paraspeckles. (A) NUN bodies are not NONO-1::GFP(+) bodies ("paraspeckles"). NONO-1::GFP(+) bodies, marked with nono-1(ot1018[nono-1::qfp::3xflaq]) are outlined in green, nucleolus and NUN bodies are outlined in white. Bar indicates 1 μm. (B) NONO-1::GFP is broadly expressed throughout the animal and is localized to nuclei. Bar indicates 100 μm. (C) Top panel: NONO-1::GFP signal is diffuse in the nucleus of early embryos at the 20-40 cell stage. Bar indicates 10 µm. Bottom panel: NONO-1::GFP nuclear foci appear in prebean embryos. Arrows point to foci. Bar indicates 10 µm. (D) NONO-1::GFP forms foci in gland (marked by #), muscle (marked by ^), and intestine (marked by *) nuclei as well as in germ cells. Bar indicates 10 µm. (E) NONO-1::GFP in hypodermal nuclei with and without transcriptional inhibition. Nucleolus outlined in pink. Bar indicates 1 µm. (F) Transcriptional inhibition resulted in less NONO-1+ bodies in hypodermal nuclei. Thick bars show median, boxes represent quartiles, and vertical lines show range. Wilcoxon signed-rank test was used. (G) Transcriptional inhibition resulted in greater NONO-1::GFP signal in the nucleoplasm hypodermal nuclei. Thick bars show median, boxes represent quartiles, and vertical lines show range. Twosample Student's t-test was used.

We used an available CRISPR/Cas9-generated reporter allele of SMN-1 (O'Hern et al. 2017), whose vertebrate ortholog SMN marks nuclear gems (Liu and Dreyfuss 1996), and found SMN-1::GFP to be absent from the nuclei of neurons (Figure 7A). SMN-1::GFP localizes to the cytoplasm in various cells (Supplementary Figure 1C, left panel). In germ cells, SMN-1::GFP localizes to foci (Supplementary Figure S1C, right panel), which are likely to be P granules based on a previous report (Barbee et al. 2002).

Similarly, we used a CRISPR/Cas9-generated GFP-tagged allele of the H3K27 histone methyltransferase complex component MES-2 (Paix et al. 2014) to assess for the presence of Polycomb bodies which contain repressed chromatin (Cheutin and Cavalli 2019; Loubiere et al. 2019; Tatavosian et al. 2019). We found that MES-2::GFP displays diffuse localization throughout the nucleoplasm (Figure 7A).

Splicing speckles, also called nuclear speckles, have classically been identified by staining against the splicing factor SC35 (Fu and Maniatis 1990). We tagged the C. elegans SC35 ortholog, RSP-4 with GFP using CRISPR/Cas9 genome engineering, to test whether NUN bodies are splicing speckles. We observed that RSP-4::GFP displays diffuse nucleoplasmic expression (Figure 7B). In addition, we GFP-tagged two alternative splicing factors, EXC-7, the C. elegans ortholog of Elav, and FOX-1, the C. elegans ortholog of the Rbfox family of splicing factors. Homologs of these two proteins in other organisms are expressed in a panneuronal manner [Drosophila Elav (Campos et al. 1987; Robinow and White 1988); Rbfox3/NeuN (Mullen et al. 1992)]. EXC-7::GFP and FOX-1::GFP factors are nuclear localized, but they display a diffuse expression throughout the nucleoplasm (Figure 7B). Moreover, we note that unlike their orthologs in other organisms, neither EXC-7 nor FOX-1 is ubiquitously expressed throughout the nervous system (Pham and Hobert 2019) (Supplementary Figure 1D).

NUN bodies are unlikely to be heterochromatin

We assessed the possibility that NUN bodies may relate to heterochromatin. Heterochromatin-associated proteins, human HP1α and Drosophila HP1, have been found to phase separate into liquid droplets in human cell lines (Larson et al. 2017) and in Drosophila embryos (Strom et al. 2017), respectively. Endogenously reported-tagged C. elegans heterochromatin-associated proteins, HPL-1 and HPL-2, show diffuse nucleoplasm expression and, therefore, no enrichment in NUN bodies (Figure 7C and data not shown).

We also considered H3K9 histone methyltransferases implicated in heterochromatin formation or spreading. We used a mCherry-tagged allele of met-2/SET1DB, generated by CRISPR/ Cas9 genome engineering (Delaney et al. 2019) but observed that MET-2::mCherry diffused throughout the nucleoplasm but concentrated at a focus on the nuclear periphery, in accordance with a recent report (Delaney et al. 2019). We also considered another H3K9 histone methyltransferase, the C. elegans ortholog of Clr4, called SET-11 (Engert et al. 2018). This protein was of specific interest because previous smFISH analysis had shown that set-11 transcripts are restricted to the nervous system (Engert et al. 2018), thereby matching the occurrence of NUN bodies. We GFP-tagged SET-11 by CRISPR/Cas9 genome engineering, but we did not detect any expression of the fusion protein.

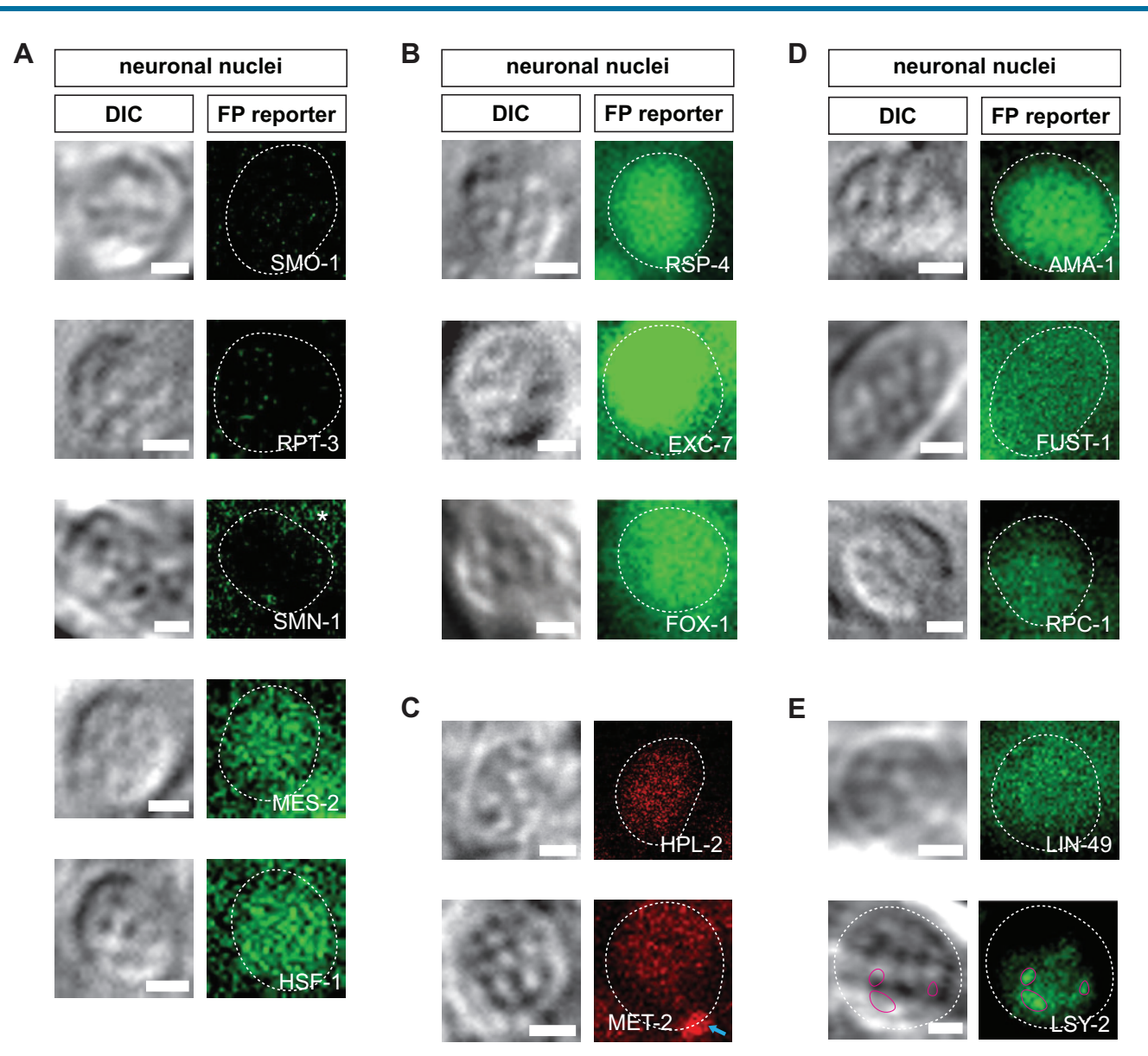


Figure 7. Co-localization studies of constituents of other nuclear bodies. (A) Nomarski micrographs of neuronal nuclei (outlined with dotted, white line) with expression of various orthologous proteins that constitute nuclear bodies in mammalian systems, SMO-1 (marked with smo-1(ot1038[smo-1::gfp::3xflag]), SMN-1 (marked with smn-1(rt280[smn-1::gfp])), RPT-3 (marked with rpt-3(ot1017[rpt-3::gfp::3xflag])), MES-2 (marked with mes-2(ax2059[mes-2::gfp])), and HSF-1 (marked with drSi13). * marks cytoplasmic expression of SMN-1::GFP. Bar indicates 1 μm. (B) Nomarski micrographs of neuronal nuclei (outlined with dotted, white line) with expression of splicing proteins, RSP-4 (marked with rsp-4(syb2575[rsp-4::gfp])) and EXC-7 (marked with exc-7(ot970[exc-7::gfp::3xflag])). Bar indicates 1 μm. (C) Nomarski micrographs of neuronal nuclei (outlined with dotted, white line) with expression of heterochromatin-associated proteins, HPL-2 and MET-2. Blue arrow points to MET-2::mCherry foci localized to the nuclear periphery. Bar indicates 1 μm. (D) Nomarski micrographs of neuronal nuclei (outlined with dotted, white line) with expression of transcription-associated proteins, AMA-1 (marked with man-1(ot1037[gfp::3xflag::aman-1])), FUST-1 (marked with fust-1(ot1039[fust-1::gfp::3xflag])), and RPC-1 (marked with images of expression of LIN-49 and LSY-9 (LSY-2::GFP+ bodies outlined in magenta). Bar indicates 1 μm. Additional expression outside the nervous system documented in Supplementary Figure S1.

We also tested whether mutations in the proteins described above affect the presence of NUN bodies. We found no effects on NUN bodies in *hpl-1*, *hpl-2* single and double mutants; *mes-2* mutants; *met-2*, *set-25* double mutants; and *set-11* mutants (Supplementary Table S2). We also note that NUN bodies are not located toward the periphery of the nucleus, where repressed chromatin is preferentially localized (Ahringer and Gasser 2018).

To be able to simultaneously visualize DNA and the NUN bodies, we used Hoechst 33342 which stains heterochromatin more intensely (Imai et al. 2017). Though there was a small proportion

(7.5%) of neuronal and glial nuclei that showed localization of the DNA dye to the NUN bodies, the NUN bodies in about two-thirds of nuclei examined did not show any co-localization with the DNA dye (Supplementary Figure S2, A and B).

We also used a SYTO RNA dye to probe the relationship of nuclear RNAs to the NUN bodies. We validated the protocol for this staining procedure by successfully staining the large, rRNA-containing nucleolus of the excretory gland cell (Supplementary Figure S2C). In the nervous system, however, the RNA dye localized to the NUN bodies only in very small proportion (2.5%) of

neuronal and glial nuclei, while in nearly 80% of nuclei observed, NUN bodies and RNA staining did not co-localize (Supplementary Figure S2, D and E). We were unable to draw any definitive conclusions from the live staining of DNA or RNA because (1) a significant proportion of nuclei were unstained for DNA (~25%) and for RNA (~18%) (Supplementary Figure S2, B and E), (2) the ability of a successful live stain may depend on staining conditions, and (3) the phase-separated nature of NUN bodies could interfere with their ability to be stained with a live stain.

Relationship of NUN bodies to other phase-separated structures

Core transcriptional machinery has recently been reported to localize to phase-separated transcriptional condensates, and those condensates contain RNA polymerase II (Cho et al. 2018; Sabari et al. 2018) and other factors, such as TAF15 (Shin et al. 2019; Wei et al. 2020). We used CRISPR/Cas9 engineering to endogenously tag an RNA polymerase II subunit, AMA-1, and the EWS/FUS/ TAF15 ortholog, FUST-1. We found that neither of these proteins were enriched in NUN bodies. Rather, they both showed a diffuse nuclear localization (Figure 7D). FUST-1 also showed diffuse cytoplasmic localization in somatic nuclei (Supplementary Figure S1G). Unexpectedly, we observed that in the germ line FUST-1 localizes to P granules (Supplementary Figure S1F).

We also used CRISPR/Cas9 to endogenously tag a RNA polymerase III subunit, RPC-1, with GFP. Animals carrying this reporter allele displayed diffuse nuclear localization in neuronal nuclei (Figure 7D) with occasional nuclear foci in hypodermal and germ cell nuclei (Supplementary Figure S1E).

Acetylated chromatin can also phase-separate, encompassing acetylated histone-binding bromodomain proteins (Gibson et al. 2019). We examined the localization of two C. elegans bromodomain proteins, LIN-49 (Chang et al. 2003) and BET-1 (Shibata et al. 2010), but both show a diffuse localization throughout the nucleoplasm (Figure 7E and data not shown).

Even though not explicitly shown to be a phase-separated structure, the Zn finger protein LSY-2 was previously shown to localize to subnuclear foci (Johnston and Hobert 2005). We find that these foci do not overlap with NUN bodies (Figure 7E).

NUN bodies are not affected by mutations in constituents of subnuclear biomolecular condensates

Lastly, we also tested whether mutations in the factors whose localization we examined above will have any effect on NUN body appearance. We examined animals carrying loss of function mutations in fib-1/Fibrillarin, mes-2/EZH2, nono-1/NONO, rsp-4/ SC35, smn-1/SMN, and smo-1/SUMO1-3 and found NUN bodies to be unaffected (Supplementary Table S2).

In yeast, a nuclear condensate comprised a Bre1 shell and a Lge1 core has been shown to promote H2B ubiquitination (Gallego et al. 2020). To test whether the NUN bodies are these orthologous condensates, CRISPR/Cas9 genome engineering was used to generate a double null allele of the C. elegans orthologs of Lge1, the adjacently located wac-1.1 and wac-1.2 loci (Supplementary Figure S3A). We observed no changes in NUN body appearance in wac-1.1, wac-1.2(syb2587) mutant animals (Supplementary Figure S3B).

NUN bodies are different from stress-induced nuclear granules

The heat shock protein HSF1 has been found to respond to stress by forming subnuclear structures termed nuclear stress granules, both in vertebrates (Biamonti and Vourc'h 2010) and in C. elegans (Morton and Lamitina 2013). We wondered whether NUN bodies may relate to such a stress response and perhaps be an indication of neurons being in a more "stressed state" than other cells. Using a previously described hsf-1::afp reagent that reveals nuclear stress granules (Morton and Lamitina 2013), we find that the HSF-1::GFP does not localize to the NUN bodies (Figure 7A).

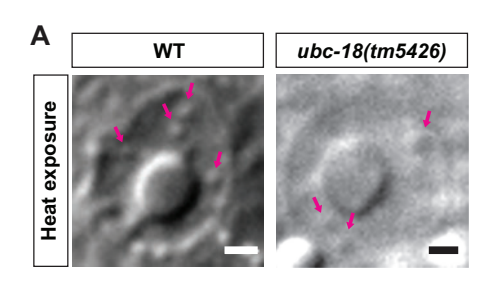
We noted that under conditions of stress, such as heat stress, non-neuronal cells also form granular structures in their nucleus that are visible by Nomarski (DIC) microscopy and appear to resemble NUN bodies observed in neurons (Figure 8A). Unexpectedly, these granules do not overlap with HSF-1::GFP granules (Figure 8B). Moreover, while previously described stressinduced nuclear granules are known to depend on ubc-18, a ubiquitin conjugating enzyme (Sampuda et al. 2017), these DICvisualized, stress-induced granules still form in non-neuronal cells in ubc-18 mutants (Figure 8A). Using the nucleolar marker FIB-1::GFP, we find these non-neuronal stress-induced granules to be nucleoli (Figure 8C). Given that neither the FIB-1::GFP nor HSF-1::GFP stress granules overlap with NUN bodies as determined by DIC microscopy (Figure 8, A and D), we infer that NUN bodies are not a reflection of stress-induced responses in neuronal nuclei.

NUN body formation in relation to neuronal differentiation programs

We asked whether and how NUN body formation relates to the execution of specific neuronal differentiation programs. As the NUN bodies are a panneuronal feature, we asked whether they are regulated by proneuronal factors that control panneuronal gene expression. The bHLH transcription factor hlh-3 acts as a proneural factor in HSNs, i.e. hlh-3 does not only affect neurontype specific features of HSN, but also controls the induction of panneuronal features (Lloret-Fernandez et al. 2018). Examining HSN by DIC microscopy in hlh-3 mutant worms, we found that the NUN bodies are unaffected (Figure 9A), suggesting that formation of NUN bodies is genetically uncoupled from the induction of panneuronal gene expression features.

The HSNs are an unusual neuron class because of a long lag between their birth and adoption of terminal differentiated features (Desai et al. 1988). The HSNs are born in embryo (Sulston et al. 1983) but only acquire terminal differentiation features, such as the expression of panneuronal markers (Figure 9B) or cell-type-specific markers (such as their serotonergic identity) in the fourth larval stage (Desai et al. 1988). We observe NUN bodies to be clearly visible at the first larval stage (Figure 9B), much before other markers of terminal differentiation of the HSNs become expressed. Similar to the HSNs, the male-specific CEM neurons are born in the embryo but express neuronal marker genes only at late larval stages (Sulston et al. 1983; Pereira et al. 2015); we find that these neurons also already contain NUN bodies at the L1 stage (data not shown). These observations again argue that NUN body formation can be uncoupled from other generic aspects of neuronal differentiation programs.

We also examined animals lacking specific terminal selectortype transcription factors, unc-3 and unc-86, which control the cell-type-specific differentiation programs of a number of distinct neuron types throughout the nervous system (Kratsios et al. 2012; Leyva-Diaz et al. 2020). We find that in these neuron types, NUN body formation is unaffected by loss of these genes (Figure 9A). This is consistent with previous observations in ADL neurons of a hlh-4 mutant (Masoudi et al. 2018) or the AIY neurons in ttx-3 mutants (Altun-Gultekin et al. 2001). Taken together, these



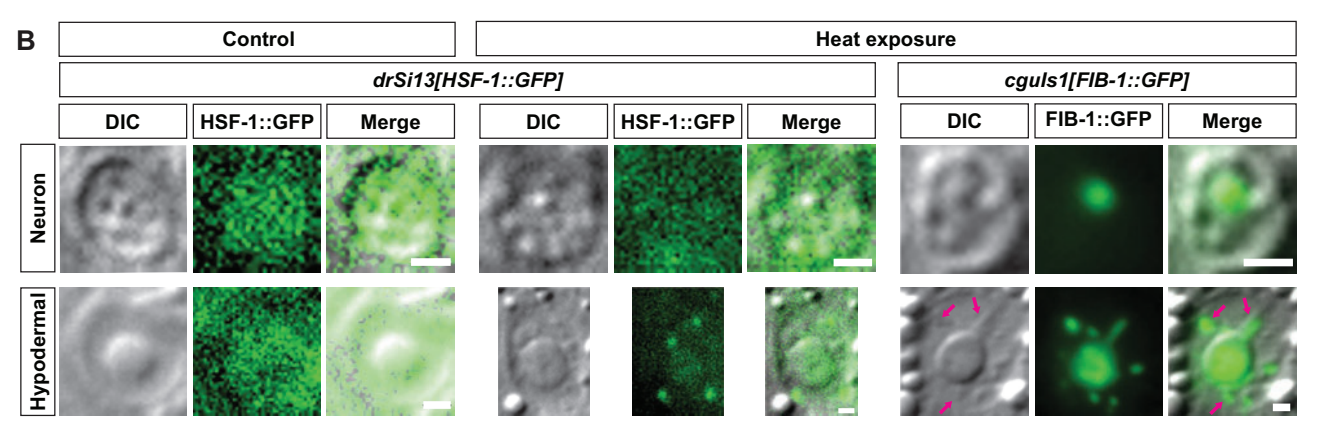


Figure 8. Stress-induced granules are different from NUN bodies. (A) Nomarski micrographs of heat stress induce granules in hypodermal nuclei in wild-type and ubc-18 mutant animals. Bar indicates 1 μ m. (B) Nomarski micrographs of neuronal and hypodermal nuclei under control and heat stress along with HSF-1::GFP and FIB-1::GFP reporters. Stress-induced granules outlined in white and co-localization with FIB-1::GFP marked with arrows. Bar indicates 1 μ m.

experiments demonstrate that the formation of NUN bodies can be genetically uncoupled from the induction of panneuronal as well as cell-type-specific differentiation programs.

CANs remodel NUN bodies during larval development

The nuclei of CANs have long been noted to have an unusual nuclear morphology (G. Giarriga, personal communication). We examined nuclear morphology of CANs at different developmental stages and observed morphological changes during larval development. At the first larval stage, CAN nuclei resemble other neuronal nuclei , displaying five to nine NUN bodies (Figure 10, A and B). However, by the L4 stage, the appearance of CAN nuclei has dramatically changed. There are on average only three nuclear granules, and they are larger than NUN bodies were in earlier stages (Figure 10A). We find that one of them is FIB-1::GFP-positive and hence a nucleolus, while the other two may represent enlarged NUN bodies (Figure 10C). Hence, the CAN cells undergo a transition in enlarging two subnuclear compartments, for reasons currently unknown.

We investigated the timing of this transition in more detail and found that in the L2 stage CANs still show NUN body appearance as in the L1 stage (data not shown). Within the first hour of the L3 stage, animals show the transition to the enlarged nuclear granules (79% of CAN nuclei transitioned, n=19). In lin-4 mutant animals, in which developmental timing decisions in multiple tissue types are maintained in the early juvenile stage (Ambros and Horvitz 1984), this transition was not affected (75% of CAN nuclei transitioned normally, n=20; Figure 10D). Additionally, we wondered whether entry into dauer development would affect this transition because the timing of this transition aligns with the development into dauers after an alternate L2 stage. However, CAN cells retain their neuron-like NUN body appearance in the dauer stage (Figure 10D). Upon recovery from dauer, the NUN bodies of

the CANs transition normally (Figure 10D). Thus, we conclude that the heterochronic and dauer pathways do not influence the transition in the NUN bodies of CAN.

Previous work has established that the Prd-type homeobox gene ceh-10 is involved in CAN cell migration and differentiation (Forrester et al. 1998; Wenick and Hobert 2004). We examined whether ceh-10 mutant animals display defects in the NUN body transformation of CANs. As null alleles of ceh-10 cause animals to arrest and die at the L1 stage (Forrester et al. 1998), we used two different hypomorphic alleles of ceh-10. In both alleles, expression of a terminal differentiation marker, kal-1, normally expressed in a number of neurons including CAN (Bülow et al. 2002) is unaffected (Figure 10E). However, in both alleles, CAN subnuclear remodeling was abrogated. The CAN nuclei retained their NUN body appearance of early larval stages and the nucleolus did not enlarge (Figure 10, A and B). We conclude that ceh-10 controls the remodeling of NUN bodies through as-yet unknown means

Discussion

We report here that NUN bodies are subnuclear organelles with an unprecedented cell type specificity. NUN bodies are tightly linked to nervous system and represent, at least to the best of our knowledge, the only feature common to all fully mature neurons and most glia. We found that NUN bodies behave as phase-separated membraneless organelles within the nucleus. We visualized components of known nuclear bodies but did not identify any fluorescently tagged proteins that localized to NUN bodies. In fact, we observe very few focal structures in the *C. elegans* nucleus. For example, we expected that GFP-tagging of the sole SC35 ortholog in *C. elegans* would reveal splicing speckles observed in other species, but we did not find this to be the case. This may reflect the much smaller size of the *C. elegans* neuronal

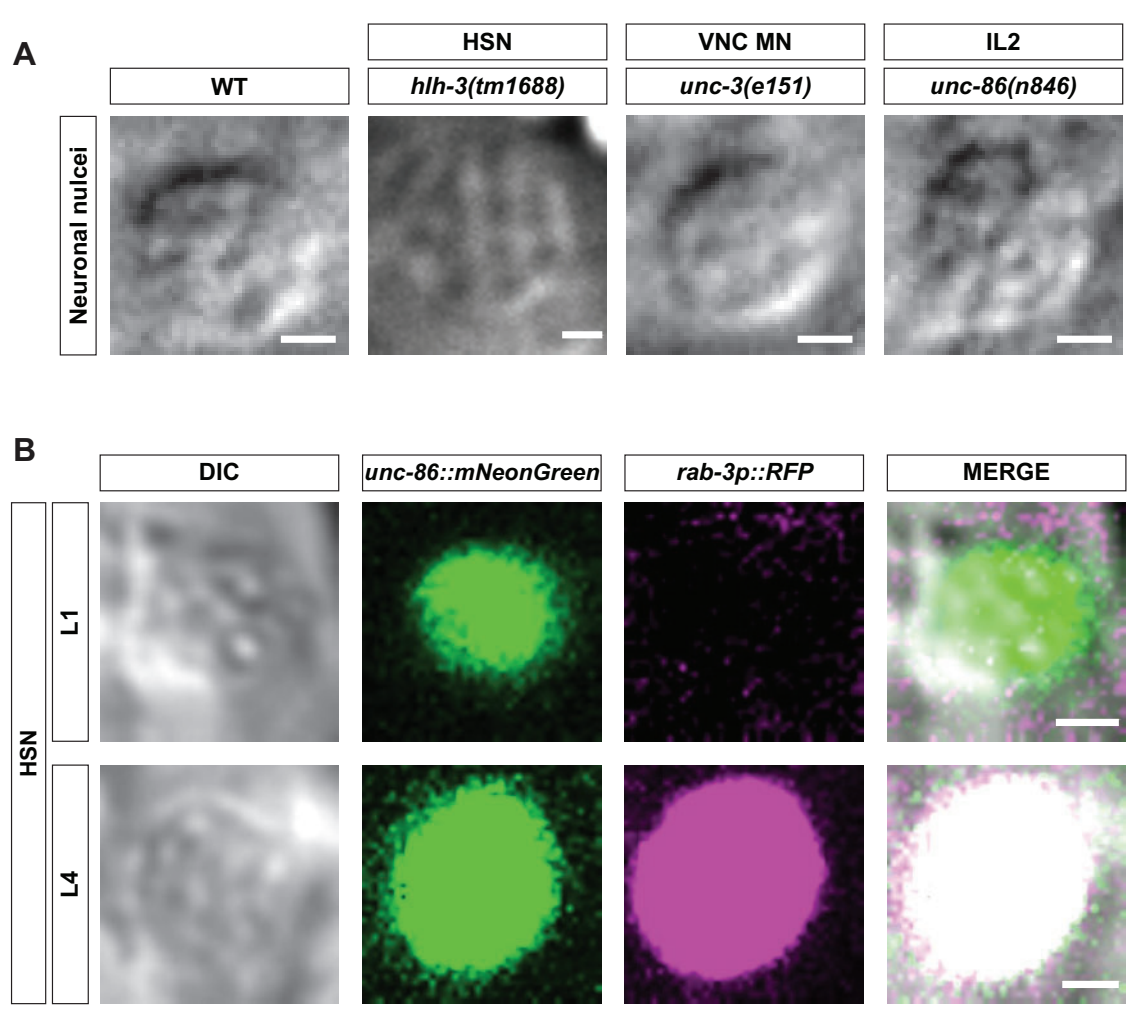


Figure 9. Relationship of NUN body formation to other neuronal differentiation events. (A) Nomarski micrographs of neuronal nuclei in proneuronal gene and terminal selector mutant animals in different cell types. Bar indicates 1 µm. (B) NUN bodies appear before panneuronal gene expression in HSN; DIC micrograph of HSN nuclei and fluorescent reporters. Bar indicates 1 µm. For quantification of NUN body number in HSN, see Figure 2D.

nucleus (\sim 2.5 μ m) compared to vertebrate nuclei which can be an order of magnitude larger. The need to compartmentalize functions into dedicated subcompartments or organelles may not manifest in nuclei of this relatively small size.

As a note of caution, we realize that GFP tagging may affect proper nuclear localization. Loss of function of the loci that we tagged displays strong phenotypes (e.g. smo-1 or mes-2 null mutants or RNAi against rpt-3 results in lethality and/or sterility). For all of the endogenous GFP tags created with CRISPR/ Cas9 genome engineering except two, we do not observe that GFP tagging resulted in obvious mutant phenotypes, leading us to infer that protein tagging does at least not affect protein function for the majority of our tagged proteins. As for the two exceptions, animals homozygous for the RPT-3::GFP allele have markedly reduced fertility, and those homozygous for the FIB-1::GFP allele are not fertile. However, our FIB-1::GFP localizes properly to the nucleolus as confirmed with an independent marker of a different nucleolar protein and as confirmed by their enlargement in ncl-1 mutant animals. Additionally, limitations in the resolution of our microscopy may interfere with our ability to observe higher concentrations of tagged protein within NUN bodies. However, the discrete nature, size and ease by which NUN bodies can be observed make such a possibility unlikely.

We also tested the hypothesis that the NUN bodies are reflective of heterochromatin, but we have found no evidence to support that hypothesis. However, our experiments are limited in their ability to rule out that NUN bodies are related to heterochromatin as a recent study has shown that the removal of H3K9me3 and HP1α did not abolish heterochromatin compartmentalization at chromocenters (Erdel et al. 2020).

As we tried to define the subnuclear compartments though qfp tagging of candidate components, we serendipitously discovered a few notable vignettes. First, we observed that the FUST-1 protein, the C. elegans homolog of a prominent human disease gene FUS1 (Zhang et al. 2018), localizes to P-granules, RNA/protein condensates in the germline (Seydoux 2018). Second, we found that the C. elegans ortholog of the vertebrate Rbfox proteins, one of which a commonly used panneuronal marker (Conboy 2017), is not panneuronal in C. elegans. Third, we found that a key component of the 26S proteasome complex, RPT-3, displays distinct subcellular localization patterns in distinct cell types. RPT-3 is excluded from the nuclei of neurons but not from the nuclei of other cell types, e.g. muscle and hypodermal cells. Fourth, despite the paucity of conserved nuclear bodies, we found that contrary to previous assumptions, C. elegans does contain paraspeckles. While the structure of the C. elegans ortholog of NONO/SFPQ/PSPC1, core constituents of paraspeckles, has previously been reported (Knott et al. 2015), the absence of clear

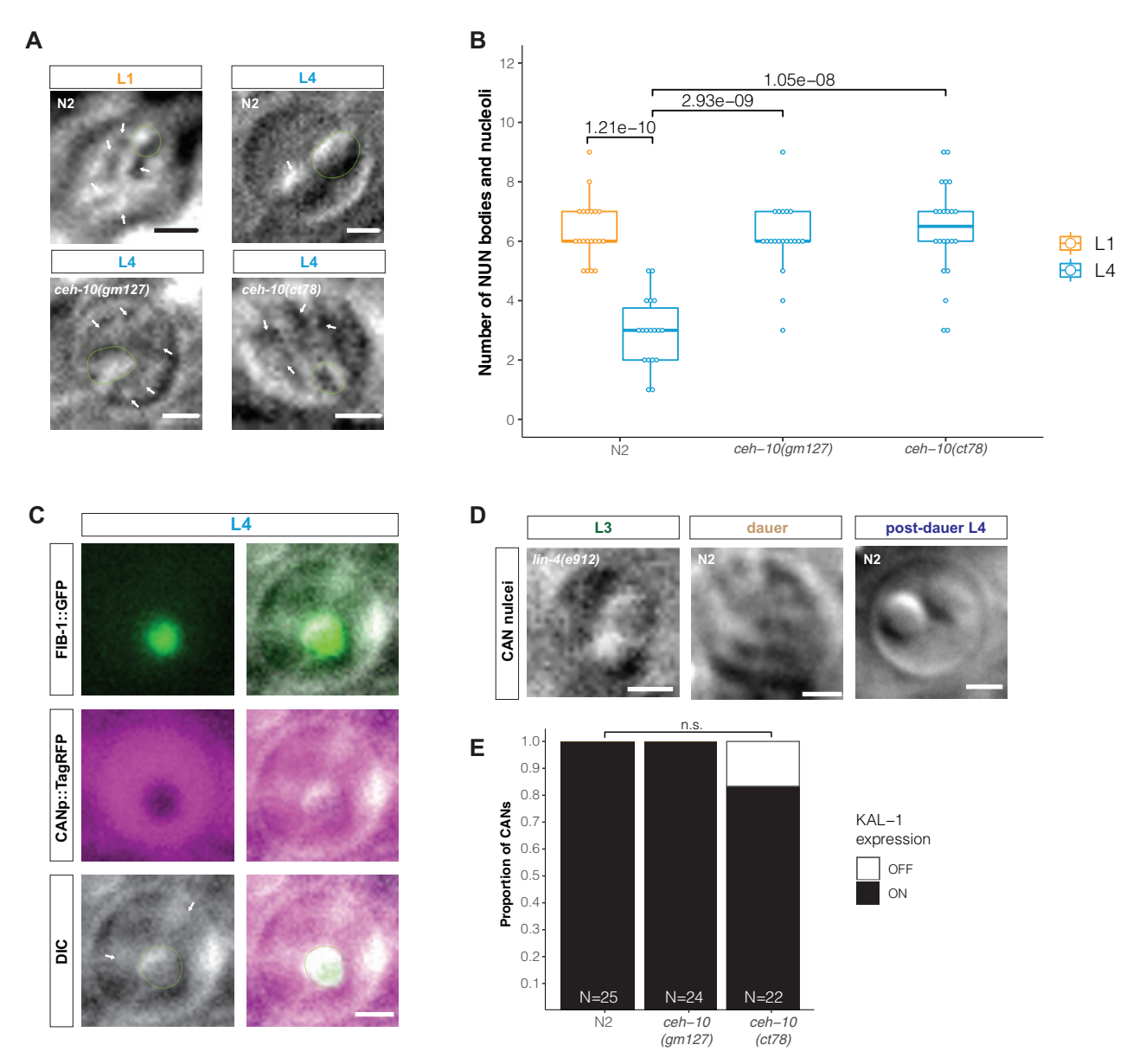


Figure 10. NUN bodies remodel in the CANs in a ceh-10-dependent manner. (A) Nomarski micrographs of CAN nuclei in wild-type and ceh-10 mutant animals. Bar indicates 1 μ m. (B) Number of NUN bodies and nucleoli in CAN nuclei in wild-type and ceh-10 mutant animals. Thick bars show median, boxes represent quartiles, and vertical lines show range. Two-sample Student's t-test was used. (C) Nomarski micrographs of CAN nucleus with nucleolus labeled by FIB-1::GFP. Nucleolus outlined in green and NUN bodies outlined in yellow. Bar indicates 1 μ m. Thick bars show median, boxes represent quartiles, and vertical lines show range. Two-sample Student's t-test was used. (D) Nomarski micrographs of CAN nucleus in lin-4(e912) L3 animal, a wild-type dauer animal and an L4 post-dauer animal. Bar indicates 1 μ m. (E) kal-1p::gfp (otIs33) reporter gene expression in CAN in wild-type and ceh-10 mutant animals.

sequence homolog of the long non-coding RNA, NEAT1, in non-mammalian vertebrates and invertebrates such as *C. elegans* had led to the suggestion that paraspeckles are mammalian specific (Fox et al. 2018; Nakagawa et al. 2018). Such argument has to be taken with caution as homologs of non-coding RNAs can be notoriously difficult to identify. We observe clear NONO-1(+) foci in the nucleus and describe behaviors of these foci that match those of canonical, mammalian paraspeckles.

As their constituents still remain undefined, NUN bodies remain a mystery, much alike many other nuclear bodies whose function has remained unknown. The most interesting aspect of NUN bodies is that they represent a unique aspect of nuclear biology that is restricted only to the nervous system. As known regulators of neuronal identity, i.e. terminal selectors and proneuronal factors, do

not regulate the formation of NUN bodies, they present an unexplored facet of nervous system identity and fate acquisition. Even though we failed to identify molecular components of NUN bodies, our detailed description of their specific features poses a fascinating riddle: What makes nuclei of cells of the nervous system different from those of cells outside the nervous system? As nuclear granules exist in all cells after they exit the cell cycle and start to differentiate, but are maintained exclusively within the nervous system, we speculate that NUN bodies are reflective of cellular differentiation events that may require increased gene expression and regulation (e.g. increased transcription or splicing), which initially occurs in all cells. The rapid appearance of NUN bodies after terminal cell division argues against the possibility that their formation requires novel protein synthesis, but NUN bodies may

assemble as conduits to enable the increased gene regulatory demands of differentiating cells as gene expression can be regulated through concentration of factors in distinct subnuclear microenvironments (Tsai et al. 2020). After an initial wave of differentiation, neurons and glia cells may retain the clustering of gene regulatory machinery as a reflection of a sustained regulatory demand. Such a sustained gene regulatory demand may be a unique feature of the nervous system.

The robust developmental appearance of the NUN bodies in the nervous system and their reorganization in the CANs offer attractive paradigms to interrogate the factors that control and modulate nuclear architecture. Ultimately, the most elegant way to gain further insights into the nature of NUN bodies may be genetic screens for mutants in which NUN bodies fail to form.

Acknowledgments

We thank Chi Chen for assistance with microinjections to generate strains, Veronika Solianova for providing the CRISPR/Cas9 engineered gfp-tagged fox-1 allele, Karolina Kaczmarczyk for taking some micrographs, Ev Yemini for nuclear size measurements, Anne Hart and Shai Shaham for sharing strains, Geraldine Seydoux for discussions, Robert H. Horvitz, Martin Chalfie, and John White for comments on the article, and the Caenorhabditis Genetics Center (CGC) [supported by the National Institutes of Health Office of Research Infrastructure Programs (P40 OD-010440)] and the National Bioresource Project for the Nematode (directed by Shohei Mitani at Tokyo Women's Medical University School of Medicine) for providing strains.

Conflicts of interest

None declared.

Literature cited

- Abraham KJ, Khosraviani N, Chan JNY, Gorthi A, Samman A, et al. 2020. Nucleolar RNA polymerase II drives ribosome biogenesis. Nature. 585:298-302.
- Ahringer J, Gasser SM. 2018. Repressive chromatin in Caenorhabditis elegans: establishment, composition, and function. Genetics. 208:
- Altun-Gultekin Z, Andachi Y, Tsalik EL, Pilgrim D, Kohara Y, et al. 2001. A regulatory cascade of three homeobox genes, ceh-10, ttx-3 and ceh-23, controls cell fate specification of a defined interneuron class in C. elegans. Development. 128:1951-1969.
- Ambros V, Horvitz HR. 1984. Heterochronic mutants of the nematode Caenorhabditis elegans. Science. 226:409-416.
- Barbee SA, Lublin AL, Evans TC. 2002. A novel function for the Sm proteins in germ granule localization during C. elegans embryogenesis. Curr Biol. 12:1502-1506.
- Bayer EA, Stecky RC, Neal L, Katsamba PS, Ahlsen G, et al. 2020. Ubiquitin-dependent regulation of a conserved DMRT protein controls sexually dimorphic synaptic connectivity and behavior. Elife. 9:e59614.
- Berry J, Weber SC, Vaidya N, Haataja M, Brangwynne CP. 2015. RNA transcription modulates phase transition-driven nuclear body assembly. Proc Natl Acad Sci U S A. 112:E5237-E5245.
- Biamonti G, Vourc'h C. 2010. Nuclear stress bodies. Cold Spring Harb Perspect Biol. 2:a000695.

- Bosher JM, Dufourcq P, Sookhareea S, Labouesse M. 1999. RNA interference can target pre-mRNA: consequences for gene expression in a Caenorhabditis elegans operon. Genetics. 153:1245-1256.
- Brenner S. 1974. The genetics of Caenorhabditis elegans. Genetics. 77: 71-94
- Bülow HE, Berry KL, Topper LH, Peles E, Hobert O. 2002. Heparan sulfate proteoglycan-dependent induction of axon branching and axon misrouting by the Kallmann syndrome gene kal-1. Proc Natl Acad Sci U S A. 99:6346–6351.
- Campos AR, Rosen DR, Robinow SN, White K. 1987. Molecular analysis of the locus elav in Drosophila melanogaster: a gene whose embryonic expression is neural specific. EMBO J. 6:425-431.
- Chalfie M, Horvitz HR, Sulston JE. 1981. Mutations that lead to reiterations in the cell lineages of C. elegans. Cell. 24:59-69.
- Chang S, Johnston RJ, Jr., Hobert O. 2003. A transcriptional regulatory cascade that controls left/right asymmetry in chemosensory neurons of C. elegans. Genes Dev. 17:2123-2137.
- Chen LL, Carmichael GG. 2009. Altered nuclear retention of mRNAs containing inverted repeats in human embryonic stem cells: functional role of a nuclear noncoding RNA. Mol Cell. 35: 467-478.
- Cheutin T. Cavalli G. 2019. The multiscale effects of polycomb mechanisms on 3D chromatin folding. Crit Rev Biochem Mol Biol. 54: 399-417.
- Cho WK, Spille JH, Hecht M, Lee C, Li C, et al. 2018. Mediator and RNA polymerase II clusters associate in transcription-dependent condensates. Science. 361:412-415.
- Ciosk R, DePalma M, Priess JR. 2006. Translational regulators maintain totipotency in the Caenorhabditis elegans germline. Science. 311:851-853.
- Conboy JG. 2017. Developmental regulation of RNA processing by Rbfox proteins. Wiley Interdiscip Rev RNA. 10.1002/wma.1398
- Delaney CE, Methot SP, Guidi M, Katic I, Gasser SM, et al. 2019. Heterochromatic foci and transcriptional repression by an unstructured MET-2/SETDB1 co-factor LIN-65. J Cell Biol. 218: 820-838
- Desai C, Garriga G, McIntire SL, Horvitz HR. 1988. A genetic pathway for the development of the Caenorhabditis elegans HSN motor neurons. Nature. 336:638-646.
- Dokshin GA, Ghanta KS, Piscopo KM, Mello CC. 2018. Robust genome editing with short single-stranded and long, partially single-stranded DNA donors in Caenorhabditis elegans. Genetics. 210:781-787.
- Duronio RJ, Marzluff WF. 2017. Coordinating cell cycle-regulated histone gene expression through assembly and function of the Histone Locus Body. RNA Biol. 14:726-738.
- Engert CG, Droste R, van Oudenaarden A, Horvitz HR. 2018. A Caenorhabditis elegans protein with a PRDM9-like SET domain localizes to chromatin-associated foci and promotes spermatocyte gene expression, sperm production and fertility. PLoS Genet.
- Entrevan M, Schuettengruber B, Cavalli G. 2016. Regulation of genome architecture and function by polycomb proteins. Trends Cell Biol. 26:511-525.
- Erdel F, Rademacher A, Vlijm R, Tünnermann J, Frank L, et al. 2020. Mouse heterochromatin adopts digital compaction states without showing hallmarks of HP1-driven liquid-liquid phase separation. Mol Cell. 78:236-249.e7.
- Fire A, Xu S, Montgomery MK, Kostas SA, Driver SE, et al. 1998. Potent and specific genetic interference by double-stranded RNA in Caenorhabditis elegans. Nature. 391:806-811.

- Forrester WC, Perens E, Zallen JA, Garriga G. 1998. Identification of Caenorhabditis elegans genes required for neuronal differentiation and migration. Genetics. 148:151-165.
- Fox AH, Nakagawa S, Hirose T, Bond CS. 2018. Paraspeckles: where long noncoding RNA meets phase separation. Trends Biochem Sci. 43:124-135.
- Fu XD, Maniatis T. 1990. Factor required for mammalian spliceosome assembly is localized to discrete regions in the nucleus. Nature. 343:437-441.
- Galganski L, Urbanek MO, Krzyzosiak WJ. 2017. Nuclear speckles: molecular organization, biological function and role in disease. Nucleic Acids Res. 45:10350-10368.
- Gall JG. 2000. Cajal bodies: the first 100 years. Annu Rev Cell Dev Biol. 16.273-300
- Gallego LD, Schneider M, Mittal C, Romanauska A, Gudino Carrillo RM, et al. 2020. Phase separation directs ubiquitination of gene-body nucleosomes. Nature. 579:592-597.
- Gambacorta M, Flenghi L, Fagioli M, Pileri S, Leoncini L, et al. 1996. Heterogeneous nuclear expression of the promyelocytic leukemia (PML) protein in normal and neoplastic human tissues. Am J Pathol. 149:2023-2035.
- Gendrel M, Atlas EG, Hobert O. 2016. A cellular and regulatory map of the GABAergic nervous system of C. elegans. Elife. 5:
- Gibson BA, Doolittle LK, Schneider MWG, Jensen LE, Gamarra N, et al. 2019. Organization of chromatin by intrinsic and regulated phase separation. Cell. 179:470-484.e21.
- Hedgecock EM, Herman RK. 1995. The ncl-1 gene and genetic mosaics of Caenorhabditis elegans. Genetics. 141:989-1006.
- Imai R, Nozaki T, Tani T, Kaizu K, Hibino K, et al. 2017. Density of heterochromatin in live orientation-independent-DIC microscopy. Mol Biol Cell. 28: 3349-3359.
- Jarriault S, Schwab Y, Greenwald I. 2008. A Caenorhabditis elegans model for epithelial-neuronal transdifferentiation. Proc Natl Acad Sci U S A. 105:3790-3795.
- Johnston RJ, Jr., Hobert O. 2005. A novel C. elegans zinc finger transcription factor, lsy-2, required for the cell type-specific expression of the lsy-6 microRNA. Development. 132:5451-5460.
- Katz M, Corson F, Keil W, Singhal A, Bae A, et al. 2019. Glutamate spillover in C. elegans triggers repetitive behavior through presynaptic activation of MGL-2/mGluR5. Nat Commun. 10:1882.
- King MR, Petry S. 2020. Phase separation of TPX2 enhances and spatially coordinates microtubule nucleation. Nat Commun. 11:270.
- Knott GJ, Lee M, Passon DM, Fox AH, Bond CS. 2015. Caenorhabditis elegans NONO-1: insights into DBHS protein structure, architecture, and function. Protein Sci. 24:2033-2043.
- Kratsios P, Stolfi A, Levine M, Hobert O. 2012. Coordinated regulation of cholinergic motor neuron traits through a conserved terminal selector gene. Nat Neurosci. 15:205-214.
- Kroschwald S, Maharana S, Simon A. 2017. Hexanediol: a chemical probe to investigate the material properties of membrane-less compartments. Matters. doi: 10.19185/matters.201702000010
- Kudron MM, Reinke V. 2008. C. elegans nucleostemin is required for larval growth and germline stem cell division. PLoS Genet. 4: e1000181.
- Lafarga M, Berciano MT, Pena E, Mayo I, Castano JG, et al. 2002. Clastosome: a subtype of nuclear body enriched in 19S and 20S proteasomes, ubiquitin, and protein substrates of proteasome. Mol Biol Cell. 13:2771-2782.
- Lamond AI, Ly T, Hutten S, Nicolas A. 2016. The nucleolus. Encyclopedia of Cell Biology, Vol. 3. p. 254-269.

- Larson AG, Elnatan D, Keenen MM, Trnka MJ, Johnston JB, et al. 2017. Liquid droplet formation by HP1alpha suggests a role for phase separation in heterochromatin. Nature. 547:236-240.
- Lee C, Sorensen EB, Lynch TR, Kimble J. 2016. C. elegans GLP-1/Notch activates transcription in a probability gradient across the germline stem cell pool. Elife. 5:e18370.
- Leyva-Diaz E, Masoudi N, Serrano-Saiz E, Glenwinkel L, Hobert O. 2020. Brn3/POU-IV-type POU homeobox genes-Paradigmatic regulators of neuronal identity across phylogeny. Wiley Interdiscip Rev Dev Biol. 9:e374.
- Liu Q, Dreyfuss G. 1996. A novel nuclear structure containing the survival of motor neurons protein. EMBO J. 15:3555-3565.
- Lloret-Fernandez C, Maicas M, Mora-Martinez C, Artacho A, Jimeno-Martin A, et al. 2018. A transcription factor collective defines the HSN serotonergic neuron regulatory landscape. Elife. 7:e32785.
- Long F, Peng H, Liu X, Kim SK, Myers E. 2009. A 3D digital atlas of C. elegans and its application to single-cell analyses. Nat Methods.
- Lorenzo R, Onizuka M, Defrance M, Laurent P. 2020. Combining single-cell RNA-sequencing with a molecular atlas unveils new markers for Caenorhabditis elegans neuron classes. Nucleic Acids Res. 48: 7119-7134.
- Loubiere V, Martinez AM, Cavalli G. 2019. Cell fate and developmental regulation dynamics by polycomb proteins and 3D genome architecture. Bioessays. 41:e1800222.
- Lundquist EA, Reddien PW, Hartwieg E, Horvitz HR, Bargmann CI. 2001. Three C. elegans Rac proteins and several alternative Rac regulators control axon guidance, cell migration and apoptotic cell phagocytosis. Development. 128:4475-4488.
- Luo S, Horvitz HR. 2017. The CDK8 complex and proneural proteins together drive neurogenesis from a mesodermal lineage. Curr Biol. 27:661-672.
- Masoudi N, Tavazoie S, Glenwinkel L, Ryu L, Kim K, et al. 2018. Unconventional function of an Achaete-Scute homolog as a terminal selector of nociceptive neuron identity. PLoS Biol. 16: e2004979.
- Matera AG. 2003. Cajal bodies. Curr Biol. 13:R503.
- Morton EA, Lamitina T. 2013. Caenorhabditis elegans HSF-1 is an essential nuclear protein that forms stress granule-like structures following heat shock. Aging Cell. 12:112-120.
- Mullen RJ, Buck CR, Smith AM. 1992. NeuN, a neuronal specific nuclear protein in vertebrates. Development. 116:201-211.
- Nakagawa S, Naganuma T, Shioi G, Hirose T. 2011. Paraspeckles are subpopulation-specific nuclear bodies that are not essential in mice. J Cell Biol. 193:31-39.
- Nakagawa S, Yamazaki T, Hirose T. 2018. Molecular dissection of nuclear paraspeckles: towards understanding the emerging world of the RNP milieu. Open Biol. 8:108150.
- O'Hern PJ, Gonçalves IDCG, Brecht J, Lopez Soto EJ, Simon J, et al. 2017. Decreased microRNA levels lead to deleterious increases in neuronal M2 muscarinic receptors in Spinal Muscular Atrophy models. Elife. 6:e20752.
- Ogg SC, Lamond AI. 2002. Cajal bodies and coilin-moving towards function. J Cell Biol. 159:17-21.
- Paix A, Wang Y, Smith HE, Lee CY, Calidas D, et al. 2014. Scalable and versatile genome editing using linear DNAs with microhomology to Cas9 Sites in Caenorhabditis elegans. Genetics. 198:1347-1356.
- Patel T, Hobert O. 2017. Coordinated control of terminal differentiation and restriction of cellular plasticity. Elife. 6:e24100.
- Pereira L, Kratsios P, Serrano-Saiz E, Sheftel H, Mayo AE, et al. 2015. A cellular and regulatory map of the cholinergic nervous system of C. elegans. Elife. 4:e12432.

- Pham K, Hobert O. 2019. Unlike Drosophila elav, the C. elegans elav orthologue exc-7 is not panneuronally expressed. MicroPubl Biol. 2019: 10.17912/micropub.biology.000189.doi: 10.17912/micropub.biologv.000189
- Robinow S, White K. 1988. The locus elav of Drosophila melanogaster is expressed in neurons at all developmental stages. Dev Biol. 126:
- Sabari BR, Dall'Agnese A, Boija A, Klein IA, Coffey EL, et al. 2018. Coactivator condensation at super-enhancers links phase separation and gene control. Science. 361:eaar3958.361:
- Sahin U, de The H, Lallemand-Breitenbach V. 2014. PML nuclear bodies: assembly and oxidative stress-sensitive sumovlation. Nucleus. 5:499-507.
- Sampuda KM, Riley M, Boyd L. 2017. Stress induced nuclear granules form in response to accumulation of misfolded proteins in Caenorhabditis elegans. BMC Cell Biol. 18:18.
- Sasaki YT, Ideue T, Sano M, Mituyama T, Hirose T. 2009. MENepsilon/beta noncoding RNAs are essential for structural integrity of nuclear paraspeckles. Proc Natl Acad Sci U S A. 106: 2525-2530.
- Sawyer IA, Sturgill D, Sung MH, Hager GL, Dundr M. 2016. Cajal body function in genome organization and transcriptome diversity. Bioessays. 38:1197-1208.
- Serrano-Saiz E, Leyva-Diaz E, De La Cruz E, Hobert O. 2018. BRN3-type POU homeobox genes maintain the identity of mature postmitotic neurons in nematodes and mice. Curr Biol. 28: 2813-2823.e2.
- Serrano-Saiz E, Poole RJ, Felton T, Zhang F, De La Cruz ED, et al. 2013. Modular control of glutamatergic neuronal identity in C. elegans by distinct homeodomain proteins. Cell. 155:659-673.
- Seydoux G. 2018. The P granules of C. elegans: a genetic model for the study of RNA-protein condensates. J Mol Biol. 430:4702-4710.
- Shen TH, Lin HK, Scaglioni PP, Yung TM, Pandolfi PP. 2006. The mechanisms of PML-nuclear body formation. Mol Cell. 24:805.
- Shibata Y, Takeshita H, Sasakawa N, Sawa H. 2010. Double bromodomain protein BET-1 and MYST HATs establish and maintain stable cell fates in C. elegans. Development. 137:1045-1053.
- Shin Y, Chang YC, Lee DSW, Berry J, Sanders DW, et al. 2019. Liquid nuclear condensates mechanically sense and restructure the genome. Cell. 176:1518.
- Shou Q, Feng L, Long Y, Han J, Nunnery JK, et al. 2016. A hybrid polyketide-nonribosomal peptide in nematodes that promotes larval survival. Nat Chem Biol. 12:770-772.
- Stefanakis N, Carrera I, Hobert O. 2015. Regulatory logic of pan-neuronal gene expression in C. elegans. Neuron. 87:733-750.

- Strom AR, Emelyanov AV, Mir M, Fyodorov DV, Darzacq X, et al. 2017. Phase separation drives heterochromatin domain formation. Nature. 547:241-245.
- Sulston JE. 1976. Post-embryonic development in the ventral cord of Caenorhabditis elegans. Philos Trans R Soc Lond B Biol Sci. 275: 287-297.
- Sulston JE, Schierenberg E, White JG, Thomson JN. 1983. The embryonic cell lineage of the nematode Caenorhabditis elegans. Dev Biol.
- Sunwoo H, Dinger ME, Wilusz JE, Amaral PP, Mattick JS, et al. 2008. MEN epsilon/beta nuclear-retained non-coding RNAs are up-regulated upon muscle differentiation and are essential components of paraspeckles. Genome Res. 19:347-359.
- Tatavosian R, Kent S, Brown K, Yao T, Duc HN, et al. 2019. Nuclear condensates of the Polycomb protein chromobox 2 (CBX2) assemble through phase separation. J Biol Chem. 294:1451-1463.
- Tsai A, Galupa R, Crocker J. 2020. Robust and efficient gene regulathrough localized nuclear microenvironments. Development. 147:dev161430.
- Tsalik EL, Niacaris T, Wenick AS, Pau K, Avery L, et al. 2003. LIM homeobox gene-dependent expression of biogenic amine receptors in restricted regions of the C. elegans nervous system. Dev Biol. 263:81-102.
- Tursun B, Patel T, Kratsios P, Hobert O. 2011. Direct conversion of C. elegans germ cells into specific neuron types. Science. 331: 304-308.
- Wan G, Fields BD, Spracklin G, Shukla A, Phillips CM, et al. 2018. Spatiotemporal regulation of liquid-like condensates in epigenetic inheritance. Nature. 557:679-683.
- Wei MT, Chang YC, Shimobayashi SF, Shin Y, Strom AR, et al. 2020. Nucleated transcriptional condensates amplify gene expression. Nat Cell Biol. 22:1187-1196.
- Wenick AS, Hobert O. 2004. Genomic cis-regulatory architecture and trans-acting regulators of a single interneuron-specific gene battery in C. elegans. Dev Cell. 6:757-770.
- Wong MC, Martynovsky M, Schwarzbauer JE. 2011. Analysis of cell migration using Caenorhabditis elegans as a model system. Methods Mol Biol. 769:233-247.
- Yemini E, Lin A, Nejatbakhsh A, Varol E, Sun R, et al. 2021. NeuroPAL: a neuronal polychromatic atlas of landmarks for whole-brain imaging in C. elegans. Cell, in press.
- Zhang T, Wu YC, Mullane P, Ji YJ, Liu H, et al. 2018. FUS regulates activity of microRNA-mediated gene silencing. Mol Cell. 69: 787-801.e8.

Communicating editor: S. Kennedy